EUROPEAN ORGANIZATION FOR NUCLEAR RESEARCH

CERN-EP/85-81
May 23rd, 1985

KAON PRODUCTION IN $\bar{p}p$-REACTIONS AT A CENTRE OF MASS ENERGY OF 540 GeV

UA5 Collaboration

Bonn[1], Brussels[2], Cambridge[3], CERN[4] and Stockholm[5]

G.J. Alner[3*], K. Alpgård[5], P. Anderer[1], R.E. Ansorge[3], B. Åsman[5], K. Böckmann[1], C.N. Booth[3], L. Burow[1], P. Carlson[5], J.-L. Chevalley[4], C. DeClercq[2], R.S. DeWolf[3], B. Eckart[1], G. Ekspong[5,4], I. Evangelou[4$], A. Eyring[1], J.-P. Fabre[4], K.A. French[3], L. Fröbel[1], C. Fuglesang[5], J. Gaudaen[2#], C. Geich-Gimbel[1], M. Gijsen[2], K. von Holt[1], R. Hospes[1], D. Johnson[2], K. Jon-And[5], Th. Kokott[1], M. Langer[1], F. Lotse[5], R. Meinke[1], Th. Müller[1], D.J. Munday[3], J.E.V. Ovens[3], J.G. Rushbrooke[3], H. Schmickler[1], F. Triantis[4$], L. Van hamme[2], Ch. Walck[5], C.P. Ward[3], D.R. Ward[3], T.O. White[3], G. Wilquet[2] and N. Yamdagni[5].

1 Physikalisches Institut der Universität Bonn, Germany
2 Inter-University Institute for High Energies (ULB-VUB), Brussels, Belgium
3 Cavendish Laboratory, Department of Physics, Cambridge University, UK
4 CERN, Geneva, Switzerland
5 Institute of Physics, University of Stockholm, Sweden

ABSTRACT

Using the UA5 detector, the inclusive central production of K^0_S and $K^{\pm}$ mesons has been measured in non single-diffractive interactions at the CERN SPS $\bar{p}p$ Collider at a c.m. energy of 540 GeV. The average transverse momentum is found to be $\langle p_T \rangle = 0.57 \pm 0.03$ GeV/c in the rapidity range $|y|<2.5$, which is an increase of about 30% over the top ISR energy. The K/π ratio has increased from about 8% at ISR energies to $9.5 \pm 0.9 \pm 0.7$% (the last error is systematic) at 540 GeV. The average number of K^0_S per non single-diffractive event is 1.1 ± 0.1 and the inclusive inelastic cross-section is estimated at 49 ± 5 mb.

* Member of Rutherford Appleton Laboratory, Chilton, Didcot, UK.
# Also at the Universitaire Instellingen Antwerpen, Antwerp, Belgium.
$ Also at the University of Ioannina, Greece.

(Submitted to Nuclear Physics B)

1. INTRODUCTION

With the start of the CERN SPS $\bar{p}p$ Collider a new energy region (centre of mass energy $\sqrt{s}$=540 GeV*) has been opened for studying hadronic interactions. In a general survey of hadronic interactions at this new energy regime we have observed non-scaling behaviour in multiplicity and rapidity distributions [2, 3]. Observation of non-scaling behaviour often points to either changing composition of produced particles or to changes in the production mechanism. In the past ten years there have been several suggestions to explain these observations and even suggestions for the existence of new phenomena [4].

The study of strange particle production provides a useful tool in understanding the production mechanisms. Observations up to ISR energies ($\sqrt{s}$=63 GeV) show that the K/π ratio increases very slowly with energy to about 8% at ISR [5-46]. Naively, it may be believed that at sufficiently high energy the production of strange quarks relative to lighter quarks is not suppressed, but in reality the observed strange particles may be the result of mechanisms for which the suppression is governed by factors other than the centre of mass energy. For example, for the strange particles coming from the decay of non-strange resonances the suppression is governed more by the mass of the resonance than by the centre of mass energy. Furthermore, the above ratio for the associated production of strange particles in the fragmentation region may be different from that of centrally produced pairs of strange particles. A study of rapidity and p_T distributions of strange particles could provide information on the production mechanisms or on the non-scaling behaviour mentioned above, perhaps through the existence of a threshold (e.g. charm production).

The average transverse momentum, $\langle p_T \rangle$, is known to increase slowly with energy up to ISR energies, the value for kaons being some 30% larger than that for pions [24]. At the Collider the UA1 experiment has shown [47] that for charged particles the average transverse momentum has increased substantially, to $\langle p_T \rangle$ = 0.424 GeV/c from $\langle p_T \rangle$ = 0.37 GeV/c [24] at the ISR. Furthermore, in the

---

* The nominal beam momentum was 270 GeV/c, but measurements give 273.0±1.4 GeV/c [1].

UA1 experiment the $\langle p_T \rangle$ has been shown to increase with event multiplicity up to a point and then to level off at higher multiplicities, the levelling-off being interpreted as a sign of a possible phase transition of hadronic matter [48-50].

Detailed measurements of kaon production exist at c.m. energies up to 63 GeV for pp [5-29] and up to 14 GeV for $\bar{p}p$ reactions [30-42]. The first results on kaons in the p_T-range 0.2-1.8 GeV/c at the Collider energy based on 2100 minimum bias events were published from this experiment [51]. Also the UA2-experiment has published results on the inclusive $K^{\pm}$ production in the p_T-range 0.4-1.1 GeV/c and for pseudorapidity $|\eta|<0.7$ [52] ($\eta = - \ell n \tan \Theta/2$, where Θ is the centre of mass angle between the particle direction and the beam axis).

This paper gives the results from the UA5 experiment on the production of neutral and charged kaons at the Collider, based on a study of the decays $K^0_S \rightarrow \pi^+\pi^-$ and $K^{\pm} \rightarrow \pi^{\pm}\pi^+\pi^-$ ($K_{\pi 3}$) from about 8000 minimum bias events observed in the UA5 streamer chambers. The increased statistics permit a more detailed study of kaon production in the rapidity region $|y| \leq 3.5$ and the p_T-range 0-3.5 GeV/c, where $y = 0.5\ \ell n\ ((E+p_L)/(E-p_L))$ is the rapidity in the c.m. system (E is the energy and p_L is the longitudinal momentum of a particle). We present results on inclusive p_T and rapidity distributions and kaon yields. Studies of dependence on charged multiplicity as well as comparisons with results at lower energies are presented.

The outline of the paper is as follows. In section 2 we describe the UA5-detector and the data analysis procedures used to obtain a clean kaon sample. In section 3 the results are presented and discussed and comparisons with other data are made. Conclusions are drawn in section 4.

2. EXPERIMENTAL PROCEDURES

2.1 Detector and data taking

For a detailed description of the detector the reader is referred to ref. [53]. Fig. 1 shows a schematic layout of the UA5 detector. It consists of two large streamer chambers, 6 m by 1.25 m by 0.5 m, placed 4.5 cm above and below the

SPS beam axis respectively, giving a geometrical acceptance for charged particles of about 95% for the pseudorapidity range $|\eta| \leq 3$, falling to zero at about $|\eta| = 5$. Each chamber is viewed by three cameras, which are equipped with mirror systems to give stereoscopic pairs of views. The two main cameras each view slightly more than half the chamber at a demagnification of 50 and the central supplementary camera views the whole chamber at a demagnification of 80. The system is triggered by large scintillation counter hodoscopes at each end covering a pseudorapidity interval of $2.0<|\eta|<5.6$. The minimum bias trigger, requiring at least one detected particle at each end of the detector, accepted (95±2)% of the inelastic, non single-diffractive events as determined by Monte Carlo simulations.

There is no magnetic field in the chambers and thus no direct momentum measurements of the charged primary particles are possible. However, the kinematics of the K^0_S and the $K_{\pi 3}$ decays allow determination of the kaon momentum once the directions of the charged decay products are seen in the chambers. The three-body decay of K^0_L with one unseen neutral outgoing particle does not allow momentum calculation. Fig. 2 depicts schematically an event and indicates the different features that we are able to measure.

Data were obtained during two different runs, the first in October- November 1981 with a Collider luminosity of about 10^{25} $cm^{-2}s^{-1}$ and the second in September 1982 when the luminosity reached about 2×10^{26} $cm^{-2}s^{-1}$. An important improvement to the detector was the change of the 0.4 mm corrugated steel beam pipe used in the first run to a 2 mm beryllium pipe for the 1982 run, giving far fewer electro-magnetic showers. Our published results on strange particles [51] are based on data from the first run while the data presented here were obtained during the second run and thus analysed under much cleaner conditions. The K^0_S data are based on 7120 minimum bias events and the event sample underlying the $K_{\pi 3}$ data includes 1133 additional events photographed with only the two central supplementary cameras.

2.2 Scanning and measurements

Two independent methods were used to find candidates for the strange particle decays $K^0_S \to \pi^+\pi^-$ and $K^\pm \to \pi^\pm\pi^+\pi^-$; namely a special visual scan of the events

on film, and software cuts applied to measured events.

2.2.1 Visual scan

A special scan of the minimum bias events for decays seen in the chamber volumes was carried out. The signature looked for was either a V, i.e. two charged tracks starting at the same point without an associated incoming track, or a C3, i.e. a charged track branching into three charged tracks. To reduce the background, mainly from photon conversions in the chamber gas characterized by small opening angles, a V had to have a projected opening angle larger than 2^{o} on the scanning table to be accepted. A photograph of an event with a V and a C3 is shown in fig. 3.

2.2.2 Software search

After the events had passed the UA5 analysis procedure [3] where all observed tracks were digitized, reconstructed in space and associated with primary or secondary vertices, special software cuts were applied to the measured data in order to find neutral two-prong or charged three-prong decays. The aim was to find tracks close to each other with their point of closest approach inside the chamber volumes. The spatial resolution did not allow an unambigous identification of decay vertices outside the chamber volumes.

2.2.3 Check scan

All V and C3 candidates found by either method were reconstructed in space, if necessary remeasured and finally checked visually using the film and a graphics display of the measurements. To be finally accepted as a K^0_S or $K_{\pi 3}$ the candidate had to pass strict cuts further described in the next section.

The efficiency for finding a decay appearing in the final sample was calculated assuming the two methods described above to be independent. The overall finding efficiency was found to be 96% for the neutral and 84% for the charged decays. No significant variation of the finding efficiency with η, y or p_T was found.

2.3 Data reduction

2.3.1 Monte Carlo techniques

Most kaons decay before they reach the chambers (K^0_S, $c\tau$=2.7 cm [54]) or after they have passed the chambers ($K_{\pi 3}$, $c\tau$=371 cm [54]). Thus the acceptance correction is large and in order to get high statistics and an estimate of systematic errors we used a simple Monte Carlo technique (MC1) to make this correction. We generated single kaons and simulated their decay in the detector. The geometrical limits of the chambers were taken into account, but interactions and measurement errors were neglected. The p_T and rapidity distributions were assumed to factorize (see section 3.1.2 below). They were generated with the same shape as the fits to the experimental results described in section 3 below and the parameters were tuned to fit the data.

To reduce background and to extract a clean kaon sample the event candidates were subject to a number of cuts. To determine most of these and to correct for remaining background the UA5 Monte Carlo program (MC2) [55, 58] was used. This program generates complete events with particle ratios and inclusive distributions tuned to fit the data. All particles are followed through the detector allowing for decays, hadronic and electromagnetic interactions as well as simulating measurement errors on the tracks.

2.3.2 The K^0_S sample

The sample of V's included decays of K^0_S, K^0_L, Λ, $\bar{\Lambda}$, photons converting in the chamber gas and other background reactions. Since the detector has no magnetic field we can not distinguish Λ from $\bar{\Lambda}$ and from now on Λ or $\bar{\Lambda}$ is denoted with only Λ.

In order to get tracks of good quality the track length was required to be greater than 15 cm in space and the track fit root mean square less than 30 μm on the film. The two tracks of a V-candidate were fitted to a common vertex using a general least squares method taking into account the measurement errors and correlations of the track parameters [56].

The background from photon conversions was reduced by requiring the opening angle of the V to be greater than 3° in space. The opening angle distributions for Monte Carlo (MC2) generated photon conversions in the chamber gas and Monte Carlo (MC2) generated K^0_S's are shown in fig. 4 where 80% of the photons are seen to be excluded by this cut alone. After all cuts are applied we estimate a 0.2% remaining contamination of photons in the final K^0_S sample.

The two-body decays of K^0_S and Λ give V's that are coplanar with the primary vertex, i.e. the plane formed by the two outgoing tracks contains the primary vertex. The coplanarity cut to separate K^0_S or Λ from K^0_L was defined by d, the perpendicular distance between the V plane and the primary vertex, and δ, the angle between the V plane and the line connecting the primary and the V vertices. In fig. 5 a geometrical picture of the parameters is given. Fig. 6a-c show scatter-plots of d versus δ for V's decaying in the chambers. Fig. 6a and b contain K^0_S and K^0_L decays, respectively, extracted from 30000 Monte Carlo (MC2) generated events and fig. 6c contains the data sample of V's based on about 7100 events. The area of each circle is proportional to the number of events in the cell. The straight line in fig. 6a-c is the adopted cut, $d(cm) \leq 4 - \delta(°)$. According to the Monte Carlo (MC2) studies only 1.9% of the true coplanar K^0_S's were lost while 72% of the acoplanar K^0_L sample was excluded. The final contamination of K^0_L in the K^0_S sample was estimated at 3.1%.

For V candidates passing the coplanarity cut a new least squares fit to a V-vertex was performed with the constraint of the V being coplanar with the primary vertex [56]. This fit produced improved track parameters of the V tracks which were used for further calculations. The z-coordinate (the z-axis is perpendicular to the chamber bases with its origin between the two chambers) of the V-vertex was required to be $|z| \geq 5.5$ cm to make sure that the V was produced inside one of the chambers.

To fulfil momentum conservation of a neutral two-body decay the V had to straddle the line between the primary and the V vertices. Once masses are assigned to the tracks of a coplanar V it is possible to compute the momenta of the incoming neutral particle and the charged decay products from the measured angles in the laboratory frame of reference. In principle it is a constrained fit with one degree of freedom (3 momenta to be determined from 4

constraint equations) but since we have already demanded coplanarity one of the momentum equations is automatically fulfilled and it is a straightforward matter to solve the equations. We get one solution for the K^0_S-hypothesis assigning π-masses to the outgoing tracks, and two solutions for the two possible Λ-hypotheses, assigning proton mass to one and π-mass to the other outgoing track and vice versa. Considering errors on the tracks from measurements we estimate the relative error in the momentum determination to be typically ±2% for K^0_S.

To reduce further the background from K^0_L the V-vertex was restricted to the volume of a cylinder around the beam axis with a radius of 40 cm. Also the proper lifetime of the neutral strange particle was restricted to be less than 10 τ where τ = 89 ps is the mean lifetime of K^0_S [54].

A quite clean K^0_S sample can be derived from the mixed K^0_S - Λ sample by exploiting their different decay kinematics. Due to the low Q-value and to the proton being much heavier than the pion, the Λ-decay tends to be very asymmetric in the laboratory frame of reference with the proton emitted forwards in the Λ-direction. Consequently interpreting all V's as K^0_S, boosting to the K^0_S rest frame will give most true Λ's rather high values of $|\cos \theta^*_K|$, whereas true K^0_S's will populate the $\cos \theta^*_K$ distribution uniformly (θ^*_K is the angle between the incoming K^0_S and the direction of the decay products in the K^0_S rest frame). This is illustrated in fig. 7 which shows our coplanar data sample together with Monte Carlo (MC2) generated K^0_S's and Λ's. The proportion and normalization of the generated K^0_S's and Λ's are chosen according to data assuming that the left hand part of the data plot contains clean K^0_S's. The dashed line corresponds to K^0_S (MC2) and the solid line to the sum of K^0_S and Λ (MC2). It turns out that almost all Λ's will have $|\cos \theta^*_K| > 0.5$ and consequently the K^0_S sample is defined as having $|\cos \theta^*_K| \leq 0.5$.

The geometrical efficiency for detecting a K^0_S in the chambers is very small for large rapidities and for small proper lifetimes (fig. 8b and 8c). Furthermore, remaining contamination from Λ's tend to simulate K^0_S with small values of proper lifetime. The K^0_S sample was therefore restricted to $|y| \leq 3.5$ and to proper lifetimes $t > 0.75\tau$.

The remaining contamination from Λ's in the final K^0_S sample was estimated to 2.1% and corrected for using the UA5 Monte Carlo program (MC2).

The probability density function for the proper lifetime of a K^0_S observed in our detector is a truncated exponential distribution

$$f(t) = \frac{e^{-t/\tau}}{e^{-t_{min}/\tau} - e^{-t_{max}/\tau}}$$

where t_{min} and t_{max} are the minimum and maximum lifetimes respectively for the detection of each K^0_S in the fiducial volume of our detector. Since $e^{-t_{max}/\tau}$ is negligible compared to $e^{-t_{min}/\tau}$ the variable $t-t_{min}$ is expected to be exponentially distributed with the slope $1/\tau$. Fig. 9 shows the distribution of $(t-t_{min})/\tau$ for our final K^0_S sample. The data show the expected exponential behaviour with a slope of one (the straight line), thus providing a valuable check of the purity of the K^0_S sample.

Using Monte Carlo (MC1) generated decays $K^0_S \rightarrow \pi^+\pi^-$ in the region $|y|<3.5$, and applying all cuts the resulting geometrical efficiency was 3.9%. Using instead the region $|y|<2.5$ we found 4.1%. Fig. 8 shows the geometrical efficiency to detect such a decay in the chambers as a function of p_T (in the region $|y|<2.5$) (a), rapidity (b) and number of proper lifetimes (in the region $|y|<2.5$) (c). The detection efficiency is found to be fairly uniform over the rapidity region considered. As expected the efficiency versus p_T is low for K^0_S in the region $p_T \leq 0.3$ GeV/c. The overall efficiency was found to be quite sensitive to the $\langle p_T \rangle$ used in MC1, e.g. varying $\langle p_T \rangle$ for K^0_S from 0.5 to 0.6 GeV/c increased the acceptance in the region $|y|<3.5$ from 3.2% to 4.1%. Using different shapes of the y-distribution did not change the acceptance appreciably, e.g. changing from a y-distribution with a flat plateau up to $|y| \leq 2.5$ and a gaussian tail of width 0.5 to a flat distribution in the whole region changed the acceptance for $|y|<3.5$ from 3.9% to 3.7%.

The trigger inefficiency caused a loss of 5% of the minimum bias events but since the lost events had low multiplicities we estimate the loss of kaons to be 1.5%. After correcting for this loss and for the branching ratio of 68.61% [54] fig. 10 shows the fully corrected proper lifetime distribution for K^0_S. The

data are seen to be consistent with the line which has the expected slope of one thus constituting a check of the adopted correction procedures.

A summary of the cuts applied to the V sample is given in table 1a. Table 2a gives the observed numbers of K^0_S in the considered rapidity ranges after the cuts were applied.

2.3.3 The $K_{\pi 3}$-sample

To get good quality of the measurements the track lengths were required to be at least 10 cm for both incoming and outgoing tracks and the track fit root mean square should be less than 30 μm on the film. The four tracks were fitted to a common vertex using a general least squares method with the constraint of the incoming track emerging from the primary vertex [56]. The scanning efficiency was low for candidates in which the angle between the outgoing tracks was small and therefore candidates for which the opening angle between any pair of outgoing tracks was less than 2° were rejected from the sample.

The main source of background to the $K_{\pi 3}$-decays is hadronic interactions of charged particles in the chamber gas. Generally the average opening angle between any pair of outgoing tracks, $\langle\alpha\rangle$, of such an interaction is bigger than that of a $K_{\pi 3}$-decay. Fig. 11a-c show distributions of $\langle\alpha\rangle$ of Monte Carlo (MC2) generated hadronic interactions and Monte Carlo (MC2) generated $K_{\pi 3}$-decays in the ranges $|\eta|<1$, $1\leq|\eta|<2$ and $|\eta|\geq 2$ respectively. The dashed lines indicate the different cuts applied in the three regions. The cuts of $\langle\alpha\rangle < 90°$, 70° and 60° exclude 61%, 81% and 85% of the interactions in the respective region.

Also for this decay it is possible to solve for the momenta of the incoming and outgoing tracks. Assigning K-mass to the incoming and π-masses to the outgoing tracks one obtains four equations from 4-momentum conservation and can thus solve for the 4 unknown momenta. The relative precision of the kaon momentum determination is estimated to be typically ±6% for $K_{\pi 3}$. If the momentum solution of one or several tracks was negative the decay candidate was rejected. Indeed Monte Carlo (MC2) studies showed that this was the case for about 67% of the hadronic threeprong interactions in the gas. The remaining contamination of hadronic interactions in the final sample was

estimated to be about 2%. A further correction of the order of 6% was applied to the $K_{\pi 3}$ sample to take into account measurement errors causing a negative solution of the momentum.

As for the K^0_S, the geometrical efficiency depends on y (fig. 8b). For $K_{\pi 3}$ we restricted ourselves to the region $|y| \leq 2.5$.

Monte Carlo (MC1) generation of the decay $K^{\pm} \rightarrow \pi^{\pm}\pi^{+}\pi^{-}$ showed that applying the cuts mentioned above results in an overall geometrical efficiency of 9.2%. Fig. 8 shows the efficiency of detecting a $K_{\pi 3}$ decay as a function of p_T (a), rapidity (b) and number of proper lifetimes (c). As can be seen from fig. 8a the $K_{\pi 3}$ sample is a complement to the K^0_S sample in the low p_T-region. For $K_{\pi 3}$ the overall efficiency was found to be less sensitive to $\langle p_T \rangle$ used in MC1 than in the case of K^0_S, e.g. an increase of $\langle p_T \rangle$ in MC1 from 0.5 to 0.6 GeV/c implied a decrease in the acceptance from 9.9% to 9.2%.

The cuts applied to the sample are summarized in table 1b and the observed number of $K_{\pi 3}$-decays used for the analysis is given in table 2a.

3. RESULTS AND DISCUSSION

3.1 Inclusive p_T-distributions

3.1.1 Production ratio of $K^{\pm}$ and K^0_S

The fully corrected p_T-distribution for K^0_S and $(K^+ + K^-)/2$ in the range $|y| \leq 2.5$ is shown in fig. 12 and given in table 3. The branching ratios used were taken from ref. [54]. The invariant cross-section is computed assuming a non single-diffractive cross-section of 43.2±1.8 mb [57, 58]. This distribution is found to be consistent with our earlier published data [51].* In the p_T region 0.35 to 1.4 GeV/c the K^0_S and $K_{\pi 3}$ data overlap and there is good agreement. Integrating the

---

* One should note that our earlier data [51] refer to the range $|\eta| \leq 3$, compared to the range $|y| \leq 2.5$ used here. A direct comparison between the sets of data is therefore not possible.

$(K^+ + K^-)/2$ and the K^0_S data points separately in this p_T range gives the value 0.96±0.22 for the production ratio $(K^+ + K^-)/(2K^0_S)$. This value is consistent with one as expected. From now on we combine our data points from K^0_S and $(K^+ + K^-)/2$ and refer to them as the K-data.

3.1.2 p_T-distributions in different rapidity intervals

In order to study the factorization between y and p_T in the kinematic region considered, we show in fig. 13a-c the p_T-distributions for the K-data in the rapidity intervals $0 \leq |y| < 0.8$ (a), $0.8 \leq |y| < 1.6$ (b) and $1.6 \leq |y| \leq 2.5$ (c) and in fig. 13d the p_T-distribution for K^0_S in the interval $2.5 < |y| \leq 3.5$.

The lines in the figures represent the fit found for the inclusive K data (table 4a) in the region $|y| \leq 2.5$ normalized to these sets of data. The form of this fit, a combination of an exponential in transverse mass and a power law, is discussed in detail in section 3.1.3. The curves are seen to well represent the data which is also born out by a χ^2 test giving the following values of χ^2/NDF for fig. 13 a-d respectively: 9.9/11, 3.1/10, 9.5/9 and 2.7/5. We draw the conclusion that y and p_T factorize.

In order to get better statistics we therefore use the K^0_S data in the region $|y| \leq 3.5$ (p_T-distribution given in table 3) and rescale them to the region $|y| \leq 2.5$ to combine them with the $K^{\pm}$ data. The scaling factor, 0.80±0.03, is calculated integrating the data points of the fully corrected K^0_S rapidity distribution discussed in section 3.2 below.

Fig. 14 shows the invariant cross-section as a funtion of p_T for our K-data in the region $|y| \leq 2.5$ (the K^0_S points are rescaled from $|y| \leq 3.5$) compared to the published UA2 data on $K^{\pm}$ ($|\eta| \leq 0.7$) [52] rescaled to account for the value of the inelastic cross-section [59]. There is good agreement between the two sets of data.

3.1.3 The form of the inclusive p_T-distribution and calculation of $\langle p_T \rangle$

The decreasing invariant cross-section for inclusive particle production is usually parametrized according to an exponential in p_T for $p_T < 1.5$ GeV/c. At ISR energies parametrizations like $\exp(Ap_T + Bp_T^2)$ were often used [25] to take

into account that the distributions are flatter for larger p_T. At the Collider the inclusive spectra of charged hadrons [47, 59], and of pions [52, 59] have been measured up to very high transverse momenta and the invariant cross-sections follow nicely a QCD inspired power law form:

$$E\frac{d^3\sigma}{d^3p} = C\frac{p_0^n}{(p_0 + p_T)^n}, \qquad (1)$$

a formula which for small values of p_T approaches $C\exp(-np_T/p_0)$.

There are few data available from high energy colliding beam experiments on the low part of the p_T-spectrum, say below 0.3 GeV/c. This region was studied in detail by one experiment at the ISR [26] where it was found that the form best fitting the data was an exponential in transverse mass m_T ($m_T^2 = m^2 + p_T^2$, m being the mass of the particle):

$$E\frac{d^3\sigma}{d^3p} = A\exp -(b\, m_T). \qquad (2)$$

It has also been pointed out by Hagedorn [49] that from a statistical point of view form (2) is more likely than a simple exponential for low p_T, being closer to a thermal Boltzmann distribution. Since our data extend right down to p_T=0 we are in a good position to study the form of the p_T-spectrum over a large range.

The p_T distribution of our K data is shown in fig. 15. The straight line is a fit to an exponential in p_T and the curve a fit with a combination of the forms (1) and (2), the changeover point between the forms being p_T= 0.4 GeV/c. The results of the fits are given in table 4a. It is clear that the power law shape (1) is preferred over the exponential at the high p_T part of the spectrum. At the low p_T part we cannot distinguish between an exponential in p_T and an exponential in m_T on grounds of χ^2 but for reasons given above we choose a combination of the forms (1) and (2) to fit the data.

In fig. 16 we compare our K data to data on charged kaon production in the central region (y=0) from the ISR ($\sqrt{s}$= 53 GeV [25]) and to the inclusive charged particle data for $|y|< 2.5$ at the Collider obtained by the UA1 experiment [47]. Our K distribution falls less steeply than that from the ISR, indicating an

increased average p_T with increasing energy. It is also less steep than the charged particle distribution from UA1 showing that also at Collider energy the $\langle p_T \rangle$ increases with increasing mass of the produced particle.

The average transverse momentum $\langle p_T \rangle$ is estimated from the fit to the combined forms (1) and (2), and has the value 0.57±0.03 GeV/c (see table 4a for details). If one varies the changeover point between forms (1) and (2) from 0 to 0.8 GeV/c the change in the resulting $\langle p_T \rangle$ is within the statistical error of ± 0.03 GeV/c. A similar fit to the ISR $K^{\pm}$-data gives $\langle p_T \rangle$ = 0.457±0.002. For comparison the UA1 experiment quotes the value $\langle p_T \rangle$ = 0.424±0.001 [47] for charged hadrons, assuming the power law form (1) to be valid for all p_T, which very likely underestimates $\langle p_T \rangle$ by some 50 MeV/c [49].

Fig. 17a shows a compilation of $\langle p_T \rangle$ for data on inclusive production of K_S^0 and $K^{\pm}$ in pp interactions [5-29] together with data points at 540 GeV from this experiment and from the UA2 experiment [52]*. One should note that the errors given are statistical only and do not take into account systematic errors varying from experiment to experiment. The $\langle p_T \rangle$ is seen to increase slowly with energy.

Fig. 17b shows the energy variation of the average transverse momentum for pions, kaon and protons. The data below 540 GeV are obtained from a compilation [24], where data from different experiments are treated in a coherent way. The straight lines are fits to the form $\langle p_T \rangle$ = a + b ℓns in the c.m. energy range 23-63 GeV. Extrapolating these fits to the Collider and comparing with the measured values shows an increase over the extrapolated value for pions [52], kaons (this experiment) and protons [52] of 14±13 %, 21±17 % and 29±19 % respectively*. In calculating the error of the overshoot at 540 GeV we took into account the systematic error of 10% in the compiled values

---

* To calculate $\langle p_T \rangle$ for the UA2 data [52] the following fits to the p_T-spectra were used. For pions we used the UA2 fit to the charged and neutral pion data [52] combined with an exponential in transverse mass for p_T<0.4 GeV/c. For kaons and protons the UA2 data cover only a limited range in p_T and exponential fits were used.

[24]. There is a suggestion of an average transverse momentum larger than a ℓns extrapolation from lower energies.

3.1.4 p_T-distributions in bands of charged multiplicity

A correlation between $\langle p_T \rangle$ and multiplicity has been found in cosmic ray data [4] and in the UA1 data on charged particles [47]. Fig. 18 shows corrected p_T-distributions for our K sample in the region $|y| \leq 2.5$ (the K^0_S data are scaled from $|y| \leq 3.5$) divided into three bands of observed charged multiplicities in the region $|\eta| \leq 3.5$, $0 \leq n_{ch} \leq 18$ (a), $19 \leq n_{ch} \leq 38$ (b) and $n_{ch} \geq 39$ (c)*. Results of fits to the combined forms (1) and (2) (the solid lines) are given in table 4b. The average p_T derived from the fit is shown in fig. 19a as a function of rapidity density. The data are consistent with an $\langle p_T \rangle$ - multiplicity correlation of similar magnitude as observed by the UA1 experiment for charged hadrons [47], also shown in the figure. The correlation is not significantly changed if instead of correlating $\langle p_T \rangle$ with the total charged multiplicity in $|\eta| \leq 3.5$ we correlate $\langle p_T \rangle$ with the local track density in a pseudorapidity region, $\Delta\eta$, centered on the kaon pseudorapidity, which can be seen from fig. 19b.

3.2 Inclusive rapidity and pseudorapidity distributions

The corrected K^0_S and $K^{\pm}$ rapidity distributions folded around zero and averaged are shown in fig. 20a. The height of the plateau of the K^0_S distribution is found to be consistent with the one of the $K^{\pm}$ distribution. This is a consistency check of the value of $\langle p_T \rangle$, 0.57±0.03 GeV/c, found for the combined kaon sample and used as input to the Monte Carlo (MC1) program to compute geometrical efficiencies. An increase of $\langle p_T \rangle$ in MC1 increases the geometrical efficiency for K^0_S and decreases it for $K^{\pm}$ (most K^0_S decay before reaching the chambers whereas most $K^{\pm}$ decay after leaving the chambers).

The distributions have a central plateau with a half width at half maximum of

---

* The central region for the charged multiplicity, $|\eta| \leq 3.5$, was chosen to be able to compute central rapidity densities comparable to the ones measured by the UA1 experiment [47] in the range $|y| < 2.5$.

approximately 3 units in rapidity. The central rapidity density is 0.16±0.02 for non single-diffractive events. Comparing the height of the charged particle pseudorapidity distribution of our non single-diffractive data to the one of our inelastic data [58], we estimate the central rapidity density for K^0_S in inelastic events to be 0.15±0.02. In fig. 21 is shown the energy dependence of the central rapidity density for K^0_S production. Shown are data from lower energy pp reactions [5-29] and our measurement at 540 GeV. The rapidity density is seen to increase smoothly with energy. The line is a fit of the form a+bℓns to lower energy pp data and our inclusive data point at 540 GeV. The result of the fit is given in table 6.

Fig. 20b displays the K^0_S and $K^{\pm}$ pseudorapidity distributions folded around zero and averaged. The charged and neutral kaon distributions are found to be consistent. The dashed line in fig. 20a and b represents the UA5 charged particle pseudorapidity distribution rescaled by 0.04, which is the ratio of the central pseudorapidity densities for the kaon data and the charged particle data [58]. The shape of the kaon distributions are similar to that of the charged particle distribution.

In fig. 20c are shown the K^0_S rapidity distributions in three bands of observed charged multiplicity in the region $|\eta|\leq 3.5$, $0\leq n_{ch}\leq 21$, $22\leq n_{ch}\leq 35$ and $n_{ch}\geq 36$. They are all consistent with having the same shape as the full distribution.

3.3 Rates and cross-sections

In table 2b are given the corrected numbers of K^0_S per event. In the range $|y|\leq 2.5$ the value $\langle n_{K^0_S}\rangle = 0.72\pm 0.06$ was calculated by integrating the fit of the combined forms (1) and (2) to the corrected p_T-distribution of the K data shown in fig. 15. For the calculation in the range $|y|\leq 3.5$ only K^0_S data were used. In this range the yield was additionally calculated from the corrected lifetime distribution in fig. 10. The two values are consistent and in table 2b their average, $\langle n_{K^0_S}\rangle = 0.92\pm 0.07$, is given. These results are consistent with the published 1981 data [51] if proper allowance is made for the different rapidity or pseudorapidity ranges used.

In table 5 we give the corrected number of K^0_S in $|y|\leq 2.5$ per observed charged

track in $|\eta|\leq 3.5$ for three bands of observed charged multiplicity in this η-range. The numbers of K^0_S are obtained from integrating the fits to the combined forms (1) and (2) shown in fig. 18. The ratio is consistent with being constant, i.e. the production of kaons is proportional to the production of charged particles.

In order to extrapolate the yield of K^0_S from the measured region $|y|\leq 3.5$ to the full phase space we have used three different methods. We have tried various types of parametrizations to fit the K^0_S rapidity distribution shown in fig. 20a: a gaussian, a flat distribution with gaussian wings and a Fermi-distribution, $[1+\exp((y-y_0)/\sigma)]^{-1}$. The fits to the rapidity distribution turn out to be somewhat unstable, since the shape of the tail is heavily dependent on the last data point. However, from the fits we estimate a K^0_S yield per event of 1.02±0.10 in the full phase space. The error includes the systematic uncertainty.

An independent estimate of the K^0_S yield in the full rapidity range was made assuming the shape of the charged particle pseudorapidity distribution, which is measured in the region $|\eta|<5$, (fig. 20a,b) to be valid also for the K^0_S distribution. Using the UA5 event generator (MC2) to correct for the differences between rapidity and pseudorapidity and to extrapolate from $|\eta|\leq 5$ to full phase space (an extrapolation of the order of 4%), we estimate the K^0_S yield per event to be 1.08±0.08.

We have made a third estimate of the yield in full phase space using the UA5 event generator (MC2) to scale the yield in $|y|\leq 3.5$. In the event generator, which is tuned to fit the measured distributions, the production characteristics of pions and kaons are assumed to be the same apart from kinematic effects. Using this method gives a number of 1.11±0.08 K^0_S per event in the full rapidity region.

The three methods give compatible results for the yield in the full phase space and our best estimate, given in table 2b, is the average value of 1.1±0.1 K^0_S per non single-diffractive event. The error includes systematic uncertainties. Using the value 48.6±1.6 mb for the inelastic cross-section [57] and the value 5.4±1.1 mb for the single-diffractive cross-section [58] and assuming the same ratio of kaons to charged particles in non single-diffractive and single-diffractive events, we estimate a value of 1.0±0.1 K^0_S per inelastic event. The

dependence on energy of the inclusive K^0_S production in pp [5-29] and $\bar{p}p$ [30-42] reactions is shown in fig 22a. Lower energy $\bar{p}p$ data are dominated by the annihilation component which is negligible at 540 GeV. We have therefore used pp data in the energy range 3.6 to 53 GeV and our inclusive data point at 540 GeV to make a fit of the form $a+b\ell ns+c(\ell ns)^2$. The line in fig. 22a shows the result of the fit and the parameters are given in table 6.

Using a value for the inelastic non single-diffractive cross-section of $\sigma_{NSD}=43.2\pm1.8$ mb [57, 58] we get a non single-diffractive cross-section for K^0_S of 48±5 mb at $\sqrt{s}=540$ GeV. Using our estimate of the single-diffractive cross-section, 5.4±1.1 mb [58], and again assuming the same ratio of kaons to charged particles in non single-diffractive and single-diffractive events, we get a single-diffractive contribution to the K^0_S cross-section of 1.3±0.5 mb and an inelastic cross-section of 49±5 mb. This is compared to lower energy data [5-42, 60] in fig. 22b. The line is again a fit to the lower energy pp data including our inclusive data point at 540 GeV to the form used in fig. 22a and the parameters are given in table 6.

3.4 K/π ratio and strangeness suppression

The K/π ratio was calculated separately in the two regions $|y|\leq3.5$ and $|y|\leq2.5$. The pion yields were obtained from the measured charged particle yields in $|\eta|\leq3.5$ and $|\eta|\leq2.5$ [61]. The measured rates of $K^\pm$ (this work) and Ξ^- [62] and the estimated rates of $p\bar{p}$ and $\Sigma^\pm$ were subtracted* and a correction for Dalitz pairs was made. The difference between pseudorapidity and rapidity was corrected for using the UA5 Monte Carlo program (MC2). The K/π ratio was found to be consistent in the two regions with an average value of 0.095±0.009±0.007 (the last error is systematic). The energy variation of this ratio is shown in fig. 23 (only statistical errors are shown) where it is compared to results at lower energies [5-29, 55, 63]. The K/π ratio is seen to increase with energy.

---

* The $p\bar{p}$ rate was estimated using a K/p ratio of 1.48±0.11 calculated from exponential fits to p_T-distributions of kaons and protons as measured by the UA2 experiment [52]. In estimating the $\Sigma^\pm$ rate we used our previously measured Λ rate [51] and the assumption $\sigma(\Lambda)=\sigma(\Sigma^++\Sigma^-+\Sigma^0)$.

Fig. 24 shows the variation of the K/π ratio, R, with the transverse momentum. We used the K^0_S and $K^\pm$ data from this experiment and the charged pion data from the UA2 experiment [52, 59]*. Also shown are the UA2 values of the ratio $K^\pm/\pi^\pm$ [52]. The full line represents central (y=0) ISR data at $\sqrt{s}$=53 GeV [25, 26]. The Collider data at $\sqrt{s}$=540 GeV are consistent with the transverse momentum variation of R seen at the ISR at $\sqrt{s}$=53 GeV. Indeed, all central ISR data on the $K^\pm/\pi^\pm$ ratio [25] in the c.m. energy range 23-63 GeV are consistent with the same transverse momentum dependence. Also bubble chamber data on K^0_S production in the c.m. energy range 11-27 GeV [13, 16, 19, 21, 23], although in a more limited transverse momentum range, show the same p_T-dependence of R.

Although the errors are large the data are consistent with an energy independent variation of R with p_T. The observed energy variation of the inclusive K/π ratio, see fig. 23, reflects therefore merely the change of the slope of the p_T-distribution, becoming less steep with increasing energy.

It is interesting to note, that in a recently reported measurement for η=0.8 at the ISR [64], the K^+/π^+ ratio was found to stay constant at 0.46 for p_T>3 GeV/c. In this case the constant value of R was interpreted [64] as being due to the fragmentation of quark-quark scattered jets. The available data on kaon production at the Collider do not allow a quantitative comparison for large values of p_T.

Finally we have estimated the strangeness suppression factor λ, defined as the ratio of the numbers of produced $s\bar{s}$ to $u\bar{u}$ or $d\bar{d}$ pairs. We have used the formula by Anisovich and Kobrinski [65] derived from a statistical quark model which takes into account the additional suppression from resonance decays. From the K/π ratio of 0.095±0.009±0.007 we get a value of 0.30±0.03±0.03 for λ (last errors are systematic), consistent with the result of Malhotra and Orava [66] who from an analysis of experimental data get an energy independent value of

---

* For p_T>0.4 GeV/c we used the published UA2 π fit [52] renormalized with +15.5% according to [59]. For p_T<0.4 GeV/c we extrapolated using an exponential in m_T.

λ=0.29±0.02. In a recent review by Wroblewski [67] various estimates of λ are shown to be consistent with a slow increase with energy. The energy dependence of λ is further discussed in references [68, 69].

4. CONCLUSIONS

We have presented results on the inclusive production of K^0_S and $K^{\pm}$ mesons in non single-diffractive $\bar{p}p$ interactions at a c.m. energy of $\sqrt{s}$=540 GeV. The measurements were made in the central region with a c.m. rapidity $|y|\leq 3.5$. We have reached the following conclusions:

(i) In overlapping kinematical regions the production cross-section for K^0_S equals that of $(K^+ + K^-)/2$. The average number of K^0_S is 1.1±0.1 per non single-diffractive event and 1.0±0.1 per inelastic event. The inclusive non single-diffractive cross-section for K^0_S is 48±5 mb, and the corresponding inelastic cross-section is 49±5 mb.

(ii) Rapidity and transverse momentum are found to factorize. The inclusive p_T-distribution is well described by an exponential in transverse mass for $p_T<0.4$ GeV/c and a power law dependence for $p_T>0.4$ GeV/c. The average transverse momentum is found to be 0.57±0.03 GeV/c.

(iii) The rapidity distribution shows a central rapidity density of 0.16±0.02 and a half width at half maximum of approximately 3 units for non single-diffractive events. The central rapidity density for all inelastic events is estimated at 0.15±0.02.

(iv) The K/π ratio is found to be consistent with an energy independent variation with p_T. The inclusive K/π ratio, however, is seen to have increased from about 8% at ISR energies to 9.5±0.9±0.7% (last error is systematic) at the Collider, where the p_T-distributions are less steep. From the

inclusive K/π ratio at the Collider we deduce a strangeness suppression factor of $\lambda=0.30\pm0.03\pm0.03$ (last error is systematic).

ACKNOWLEDGEMENTS

We are indebted to the many members of the CERN staff, particularly from the SPS and EF Divisions, who have contributed to the success of the SPS Collider and of our experiment. We acknowledge with thanks the financial support of the Brussels group by the National Foundation for Fundamental Research and the Inter-University Institute for Nuclear Sciences, of the Bonn group by the Bundesministerium für Wissenschaft und Forschung, of the Cambridge group by the UK Science and Engineering Research Council, and of the Stockholm group by the Swedish Natural Science Research Council. Last, but not least, we acknowledge the contribution of the engineers, scanning and measuring staff of all our laboratories.

REFERENCES

[1] B. de Raad and W.C. Middelkoop, as quoted in M. Bozzo et al., Phys. Lett. 147B (1984) 385.

[2] UA5 Collab., G.J. Alner et al., Phys. Lett. 138B (1984) 304.

[3] UA5 Collab., K. Alpgård et al., Phys. Lett. 107B (1981) 310.

[4] C.M.G. Lattes et al., Phys. Rep. 65 (1980) 151.

[5] R.L. Eisner et al., Nucl. Phys. B123 (1977) 361 (pp, p_{lab}=6 GeV/c).

[6] V. Blobel et al., Nucl. Phys. B69 (1974) 454 (pp, p_{lab} at 12 and 24 GeV/c).

[7] H. Fesefeldt, Thesis, Internal Report, DESY-F1-73/11 (1973) (pp, p_{lab} at 12 and 24 GeV/c).

[8] K. Jaeger et al., Phys. Rev. D11 (1975) 1756 (pp, p_{lab}=12.4 GeV/c).

[9] B.Y. Oh and G.A. Smith, Nucl. Phys. B49 (1972) 13 (pp, p_{lab} 13-28 GeV/c).

[10] K. Alpgård et al., Nucl. Phys. B103 (1976) 234 (pp, p_{lab}=19 GeV/c).

[11] P. Aahlin et al., Physica Scripta 21 (1980) 12 (pp, p_{lab}=19 GeV/c).

[12] J. Bartke et al., Nuovo Cimento 29 (1963) 8 (pp, p_{lab}=24.5 GeV/c).

[13] V.V. Ammosov et al., Nucl. Phys. B115 (1976) 269 (pp, p_{lab}=69 GeV/c).

[14] M. Alston-Garnjost et al., Phys. Rev. Lett. 35 (1975) 142 (pp, p_{lab}=100 GeV/c).

[15] J.W. Chapman et al., Phys. Lett. 47B (1973) 465 (pp, p_{lab}=102 GeV/c).

[16] D. Brick et al., Nucl. Phys. B164 (1980) 1 (pp, p_{lab}=147 GeV/c).

[17] K. Jaeger et al., Phys. Rev. D11 (1975) 2405 (pp, p_{lab}=205 GeV/c).

[18] A. Sheng et al., Phys. Rev. D11 (1975) 1733 (pp, p_{lab}=300 GeV/c).

[19] F. LoPinto et al., Phys. Rev. D22 (1980) 573 (pp, p_{lab}=300 GeV/c).

[20] F.T. Dao et al., Phys. Rev. Lett. 30 (1973) 1151 (pp, p_{lab}=303 GeV/c).

[21] EHS-RCBC Collab., M. Asai et al., Z. Phys. C27 (1985) 11 (pp, p_{lab}=360 GeV/c).

[22] R.D. Kass et al., Phys. Rev. D20 (1979) 605 (pp, p_{lab}=400 GeV/c).

[23] H. Kichimi et al., Phys. Rev. D20 (1979) 37 (pp, p_{lab}=405 GeV/c).

[24] A.M. Rossi et al., Nucl. Phys. B84 (1975) 269 (and references therein, pp, $\sqrt{s}$ 3-53 GeV).

[25] B. Alper et al., Nucl. Phys. B100 (1975) 237 (pp, $\sqrt{s}$ 23-63 GeV).

[26] K. Guettler et al., Nucl. Phys. B116 (1976) 77 (pp, $\sqrt{s}$ 23-63 GeV).

[27] F.W. Büsser et al., Phys. Lett. 61B (1976) 309 (pp, $\sqrt{s}$ 30.6-57.7 GeV).

[28] D. Drijard et al., Z. Phys. C9 (1981) 293 (pp, $\sqrt{s}$=52.5 GeV).

[29] D. Drijard et al., Z. Phys. C12 (1982) 217 (pp, $\sqrt{s}$=63 GeV).

[30] B.Y. Oh et al., Nucl. Phys. B51 (1973) 57 ($\bar{p}p$, p_{lab} 1.09-3.45 GeV/c).

[31] S. Banerjee et al., Nucl. Phys. B150 (1979) 119 ($\bar{p}p$, p_{lab}=3.6 GeV/c).

[32] M.T. Regan et al., Nucl. Phys. B141 (1978) 65 ($\bar{p}p$, p_{lab} at 4.6 and 9.1 GeV/c).

[33] G.D. Patel et al., Z. Phys. C12 (1982) 189 ($\bar{p}p$, p_{lab}=7.3 GeV/c).

[34] D. Bertrand et al., Nucl. Phys. B128 (1977) 365 ($\bar{p}p$, p_{lab}=12 GeV/c).

[35] P. Johnson, Nucl. Phys. B173 (1980) 77 ($\bar{p}p$, p_{lab}=12 GeV/c).

[36] P.D. Gall, Thesis, Internal Report, DESY F1-76/02 (1976) ($\bar{p}p$, p_{lab}=12 GeV/c).

[37] F.T. Dao et al., Phys. Lett. 51B (1974) 505 ($\bar{p}p$, p_{lab}=14.75 GeV/c).

[38] B.V. Batyunya et al., Univ. of Helsinki, Report Series in Physics, HU-P-229 (1983) ($\bar{p}p$, p_{lab}=22.4 GeV/c).

[39] C. Poiret, et al., Z. Phys. C11 (1981) 1 ($\bar{p}p$, p_{lab}=32 GeV/c).

[40] J. Lemmone et al., Z. Phys. C24 (1984) 103 ($\bar{p}p$, p_{lab}=70 GeV/c).

[41] D.R. Ward et al., Phys. Lett. 62B (1976) 237 ($\bar{p}p$, p_{lab}=100 GeV/c).

[42] R. Raja et al., Phys. Rev. D15 (1977) 627 ($\bar{p}p$, p_{lab}=100 GeV/c).

[43] J.W. Chapman et al., Phys. Lett. 47B (1973) 465.

[44] H. Blumenfeld et al., Phys. Lett. 45B (1973) 525.

[45] T. Kafka et al., Phys. Rev. D19 (1979) 76.

[46] R. Bailly et al., Z. Phys. C22 (1984) 119.

[47] UA1 Collab., G. Arnison et al., Phys. Lett. 118B (1982) 167.

[48] J. Rafelski, "Strangeness Production in the Quark Gluon Plasma", CERN/TH 3745 (1983).

[49] R. Hagedorn, Rev. Nuovo Cimento 6 (1983) Numero 10.

[50] L. van Hove, Phys. Lett. 118B (1982) 138.

[51] UA5 Collab., K. Alpgård et al., Phys. Lett. 107B (1982) 65.

[52] UA2 Collab., M. Banner et al., Phys. Lett. 122B (1983) 322.

[53] UA5 Collab., Physica Scripta 23 (1981) 642.

[54] Particle Data Group, Revs. Mod. Phys. 56 (1984) 1.

[55] A.R. Weidberg, Thesis, University of Cambridge (1982).

[56] K. Jon-And and Ch. Walck, Univ. of Stockholm, Internal Report (to appear).

[57] UA4 Collab., M. Bozzo et al., Phys. Lett. 147B (1984) 392.

[58] UA5 Collab., Phys. Rep., to be submitted.

[59] UA2 Collab., M. Banner et al., "Inclusive Particle Production in the Transverse Momentum Range between 0.25 and 40 GeV/c at the CERN Sp$\bar{p}$S Collider", DPhPE 84-07.

[60] A. Breakstone et al., Phys. Rev. D30 (1984) 528.

[61] UA5 Collab., G.J. Alner et al., "An Investigation of Multiplicity Distributions in Different Psuedorapidity Intervals in $\bar{p}p$ Reactions at a C.M.S. Energy of 540 GeV", to be submitted to Phys. Lett..

[62] UA5 Collab., G.J. Alner et al., Phys. Lett. 151B (1985) 309.

[63] UA5 Collab., K. Alpgård et al., Phys. Lett. 112B (1982) 183.

[64] A. Breakstone et al., Phys. Lett. 135B (1984) 510.

[65] V.V. Anisovich and M.N. Kobrinski, Phys. Lett. 52B (1974) 217.

[66] P.K. Malhotra and R. Orava, Z. Phys. C17 (1983) 84.

[67] A. Wroblewski, Proceedings of the 14th International Symposium on Multiparticle Dynamics, Lake Tahoe 1983, (World Science, Singapore 1983) p. 573.

[68] K. Böckmann, "Particle production in $p\bar{p}$ interactions at 540 GeV and strange quark suppression", BONN-HE-83-18.

[69] Th. Müller, Proceedings of the 14th International Symposium on Multiparticle Dynamics, Lake Tahoe 1983, (World Science, Singapore 1983).

TABLE CAPTIONS

Table 1 Criteria to be fulfilled to be accepted as a kaon, for K^0_S (a) and $K_{\pi 3}$ (b).

Table 2 Kaon yields, observed numbers (a) and corrected numbers (b). The quoted errors are statistical only.

Table 3 The invariant cross-section for neutral (a) and charged (b) kaons as a function of p_T. The errors given are statistical only. We estimate a systematic scale error of about 5%.

Table 4 Results of fits to p_T distributions ($f = 1/\sigma\ d\sigma/dp_T^2$).
Forms used:

$$\left.\begin{array}{ll} (1)\ f \propto C\ \dfrac{p_0^{\,n}}{(p_0+p_T)^n} & p_T>0.4\ \text{GeV/c} \\ (2)\ f \propto A \exp(-b\ m_T) & p_T\leq 0.4\ \text{GeV/c} \end{array}\right\}\ \text{and}$$

(3) $f \propto A \exp(-b\ p_T)$.

When combining forms (1) and (2) the parameters A, p_0 and n are fitted. The parameters C and b are given by requiring continuity of the curve and its slope and take the values C=9.87 and b=7.43 for the case of UA5 K data in $|y|\leq 2.5$ with rescaled K^0_S data.
Data sets used: (a) UA5 kaon data in accessible y-ranges and ISR data [25] and (b) UA5 data in bands of observed charged multiplicity in the range $|\eta|\leq 3.5$.

Table 5 Kaon yields in $|y|\leq 2.5$ per observed charged track in the region $|\eta|\leq 3.5$ in bands of observed charged multiplicity in this region.

Table 6 Results of fits of the form $a + b\ \ell ns + c\ (\ell ns)^2$ to the energy dependence of experimental values of $1/\sigma_{inel}\ d\sigma/dy|_{y=0}$ (c kept fixed at zero), $\langle n_{K^0_S} \rangle$ and $\sigma(K^0_S)$ from pp data in the energy range 3.6 to 53 GeV and our inclusive result at 540 GeV.

Table 1

(a) K^0_S	
length of each track	$\geq$ 15 cm
track fit RMS	$\leq$ 30 μm
opening angle	$\geq$ 3 degrees
coplanarity cut (fig. 6)	d(cm) $\leq$ 4 - δ(degrees)
abs. value of z-coordinate	$\geq$ 5.5 cm
straddling	yes
distance between decay vertex and beam axis	$\leq$ 40 cm
proper lifetime	$\geq$ 0.75 τ $\leq$ 10 τ
$\lvert\cos\theta^*_K\rvert$	$\leq$ 0.5
abs. value of rapidity	$\leq$ 3.5

(b) $K_{\pi 3}$	
length of each track	≥ 10 cm
track fit RMS	≤ 30 μm
opening angle for each pair of outgoing tracks	≥ 2 degrees
average opening angle	
for $\|\eta\|<1$	≤ 90 degrees
for $1\leq\|\eta\|<2$	≤ 70 degrees
for $\|\eta\|\geq 2$	≤ 60 degrees
momentum of incoming and outgoing particles	> 0
abs. value of rapidity	≤ 2.5

Table 2

(a) observed numbers			
	K^0_S		$K^{\pm}$
	$\|y\|\leq 2.5$	$\|y\|\leq 3.5$	$\|y\|\leq 2.5$
min. bias events	7120	7120	8253
no of decays used	171	204	53

(b) corrected numbers*			
	$\|y\|\leq 2.5$	$\|y\|\leq 3.5$	full phase space
$\langle n_{K^0_S} \rangle$	0.72 ±0.06	0.92±0.07	1.1±0.1**
K/π ratio	0.095±0.009		

* By assumption $\sigma(K^0_S) = 0.5\ (\sigma(K^+)+\sigma(K^-))$.

** Both statistical and systematic errors are included.

Table 3

(a)		
p_T (GeV/c)	E $d^3\sigma/d^3p$ (mb $GeV^{-2}c^3$)	E $d^3\sigma/d^3p$ (mb $GeV^{-2}c^3$)
	K^0_S $\|y\|\leq 2.5$	K^0_S $\|y\|\leq 3.5$
0.425	1.66 ±0.59	1.78 ±0.52
0.55	2.73 ±0.62	2.69 ±0.53
0.65	1.53 ±0.36	1.36 ±0.29
0.75	0.89 ±0.22	0.82 ±0.18
0.85	0.68 ±0.17	0.52 ±0.12
0.975	0.28 ±0.07	0.26 ±0.06
1.125	0.17 ±0.05	0.17 ±0.04
1.275	0.13 ±0.04	0.11 ±0.03
1.425	0.090 ±0.028	0.066 ±0.020
1.6	0.031 ±0.013	0.032 ±0.012
1.85	0.031 ±0.010	0.024 ±0.007
2.25	0.012 ±0.004	0.010 ±0.003
3.0	0.0018±0.0010	0.0016±0.0009

(b)

p_T (GeV/c)	E $d^3\sigma/d^3p$ (mb $GeV^{-2}c^3$)
	$(K^+ + K^-)/2$ $\lvert y\rvert \leq 2.5$
0.1	11.3 ±2.8
0.3	4.5 ±1.0
0.5	2.23±0.67
0.8	0.30±0.17
1.2	0.22±0.16

Table 4

(a)

UA5 data fitted to form (3)

data	parameters			$\langle p_T \rangle$ (GeV/c)	$\langle n_{K^0_S} \rangle$	χ^2/NDF
	A ($GeV^{-2}c^2$)	b $(GeV/c)^{-1}$				
K, $\|y\| \leq 2.5$, K^0_S rescaled from $\|y\| \leq 3.5$	4.12±0.75	3.52±0.20		0.57±0.03	0.66±0.06	24.3/16

UA5 data fitted to the combined forms (1) and (2)

data	parameters			$\langle p_T \rangle$ (GeV/c)	$\langle n_{K^0_S} \rangle$	χ^2/NDF
	A ($GeV^{-2}c^2$)	n	p_0 (GeV/c)			
K, $\|y\| \leq 2.5$	127±41	7.97±0.55	1.30±0.16	0.57±0.03	0.69±0.06	20.4/15
K, $\|y\| \leq 2.5$ K^0_S rescaled from $\|y\| \leq 3.5$	133±46	8.29±0.49	1.37±0.16	0.57±0.03	0.72±0.06	18.1/15
K^0_S, $\|y\| \leq 3.5$	119±51	10.42±0.67	1.99±0.24	0.58±0.04	0.90±0.11	11.5/10

$(K^+ + K^-)/2$ at $\sqrt{s}$=53 GeV [25] fitted to the combined forms (1) and (2)

K charged y=0	296±12 (mb $GeV^{-2}c^3$)	15.17±0.14	2.52±0.03	0.457±0.002		34.6/17

(b) UA5 K data in $|y|\leq 2.5$ (K^0_S rescaled from $|y|\leq 3.5$) fitted to the combined forms (1) and (2) (the parameter p_0 is kept at a fixed value of 1.4 GeV/c)

n_{ch}, $\|\eta\|\leq 3.5$	$n_{ch}/\Delta\eta$	parameters		$\langle p_T \rangle$ (GeV/c)	$\langle n_{K^0_S} \rangle$	χ^2/NDF
		A ($GeV^{-2}c^2$)	n			
0 - 18	1.67±0.01	99± 42	8.90±0.50	0.52±0.04	0.40±0.04	15.1/8
19 - 38	3.81±0.01	80± 32	7.68±0.46	0.64±0.06	0.70±0.09	11.5/9
39 -	6.93±0.04	248±107	7.98±0.51	0.61±0.05	1.78±0.26	5.9/9

Table 5

n_{ch} in $\|\eta\|\leq 3.5$	$\langle n_{K^0_S} \rangle / \langle n_{ch} \rangle$
0 - 18	0.034±0.003
19 - 38	0.026±0.003
39 -	0.037±0.005
all	0.034±0.003

Table 6

data	parameters			χ^2/NDF
	a	b	c	
$1/\sigma\ d\sigma/dy$ at y=0	−0.035±0.002	0.015±0.001	0 (fixed)	30/12
$\langle n_{K^0_S} \rangle$	0.014±0.004	−0.028±0.002	0.0094±0.0003	95/22
$\sigma\ (K^0_S)$	0.93 ±0.12	−1.18 ±0.07	0.34 ±0.01	98/22

FIGURE CAPTIONS

Fig. 1 Schematic lay-out of the UA5-detector.

Fig. 2 Schematic picture of an event as detected in the streamer chambers. The items in parentheses indicate what features we are able to measure for the various particles.

Fig. 3 Photo of an event as seen in one of the streamer chambers. The arrows point to the decays of a K^0_S and a $K_{\pi 3}$ respectively.

Fig. 4 Distribution of opening angles for Monte Carlo (MC2) generated photon conversions in the chamber gas (the dashed histogram) and Monte Carlo (MC2) generated K^0_S decays (the solid line histogram). The dashed line indicates the opening angle cut.

Fig. 5 Geometrical picture of the parameters d and δ used to define the coplanarity cut.

Fig. 6 Scatter plot of d versus δ for Monte Carlo (MC2) generated K^0_S (a), Monte Carlo (MC2) generated K^0_L (b) and the data sample of V's (c). The area of each circle is proportional to the number of events in the cell. Plots (a) and (b) have the same scale, the largest circle corresponding to 1912 events. The largest circle in plot (c) corresponds to 379 events. The lines indicate the coplanarity cut described in the text.

Fig. 7 The histogram shows the distribution of $|\cos \Theta^*_K|$ for the data sample of coplanar V's. The dashed line corresponds to Monte Carlo (MC2) generated K^0_S's and the full line to the sum of Monte Carlo generated K^0_S's and Λ's, the proportions of which are explained in the text.

Fig. 8 Curves showing the geometrical efficiency, ε_G, for $K^\pm$ and K^0_S, after applying all cuts, plotted as a function of

p_T (a), rapidity (b) and number of lifetimes (c).

Fig. 9 Distribution of the proper time spent inside the fiducial volume for the observed K^0_S's. The line has the expected slope of 1.

Fig. 10 Fully corrected proper lifetime distribution for the K^0_S sample. The line has the expected slope of 1.

Fig. 11 Distributions of the average opening angle for Monte Carlo (MC2) generated hadronic threeprong interactions in the streamer chamber gas (the dashed histograms) and Monte Carlo (MC2) generated $K_{\pi 3}$ decays (the solid line histogram) in the regions $|\eta| \leq 1$ (a), $1 < |\eta| \leq 2$ (b) and $|\eta| > 2$ (c). The dashed lines indicate the adopted cuts in the three regions.

Fig. 12 Inclusive p_T-distribution for $(K^+ + K^-)/2$ and K^0_S in the region $|y| \leq 2.5$.

Fig. 13 Inclusive p_T-distributions for $(K^+ + K^-)/2$ and K^0_S in the regions $|y| < 0.8$ (a), $0.8 \leq |y| < 1.6$ (b), $1.6 \leq |y| \leq 2.5$ (c) and $2.5 < |y| \leq 3.5$ (d). The curves in (a) to (d) have all the same shape given by the fit to the inclusive K data in $|y| \leq 2.5$, but they are normalized to each set of data.

Fig. 14 The invariant cross-section plotted as a function of p_T for $(K^+ + K^-)/2$ and K^0_S measured in this experiment in the range $|y| \leq 2.5$ (the neutral kaons are rescaled from the region $|y| \leq 3.5$) and for $(K^+ + K^-)/2$ measured by the UA2 experiment in the range $|\eta| < 0.7$ [52, 59].

Fig. 15 Inclusive p_T-distribution for $(K^+ + K^-)/2$ and K^0_S in the region $|y| \leq 2.5$ (the neutral kaons are rescaled from the region $|y| \leq 3.5$). The lines are fits described in the text.

Fig. 16 The invariant cross-section plotted as a function of p_T. The circles represent kaon data measured in this experiment and

the curve through them is a fit described in the text. $(K^+ + K^-)/2$ data from ISR at $\sqrt{s}$=53 GeV [25] are represented by a fit to the same shape. The UA1 inclusive charged hadron data are represented by the fit in ref. [47].

Fig. 17 (a) The dependence of $\langle p_T \rangle$ on c.m. energy for kaon data. Data below 540 GeV are from references [5-29]. The open triangle at 540 GeV is an estimate of $\langle p_T \rangle$ from a fit described in the text to UA2 data [52].
(b) The dependence of $\langle p_T \rangle$ on c.m. energy for pions, kaons and protons. Data below 540 GeV are from ref. [24] (the error in each point is assumed to be 5%). At 540 GeV the pion, kaon (other than UA5) and proton points are estimated from fits, described in the text, to UA2 data [52].

Fig. 18 Inclusive p_T distributions for kaons in three bands of observed charged multiplicities in the region $|\eta| \leq 3.5$, $n_{ch} \leq 18$ (a), $19 \leq n_{ch} \leq 38$ (b) and $n_{ch} \geq 39$ (c). The curves are results of fits to the combined forms (1) and (2) (table 4b).

Fig. 19 (a) $\langle p_T \rangle$ for our K data and UA1 data [47] on charged hadrons plotted as a function of charged particle rapidity density. We have estimated the rapidity density as the observed number of charged particles per unit of pseudorapidity in the region $|\eta| \leq 3.5$. The charged particle data from ref. [47] are measured in the region $|y| < 2.5$.
(b) $\langle p_T \rangle$ for our K data plotted versus pseudorapidity density in the interval $|\eta| \leq 3.5$ and in the intervals $\Delta\eta = 1$ and $\Delta\eta = 2$ centered on the kaon pseudorapidity. One should note that the 3 sets of points are correlated.

Fig. 20 Inclusive rapidity (a) and pseudorapidity (b) distributions for kaons. The dashed lines represent the UA5 charged particle pseudorapidity distribution rescaled by the K^0_S/charged ratio of 0.04.
(c) Rapidity distributions for kaons in bands of observed

charged multiplicity in the region $|\eta|\leq 3.5$.

Fig. 21 The c.m. energy dependence of the central rapidity density for inclusive K^0_S data. Also plotted is our non single-diffractive measurement. The data points other than UA5 are estimated from diagrams in references [5-29]. The line is a fit described in the text.

Fig. 22 The c.m. energy dependence of the inclusive K^0_S yield (a) and the inclusive K^0_S cross-section (b). Also plotted is our measurement of the K^0_S yield in non single-diffractive events. Data points other than UA5 are from references [5-42]. The cross-section point covering the range 30.4-62.2 GeV is an average value estimated from ref. [60]. The lines are fits described in the text.

Fig. 23 The c.m. energy dependence of the K/π ratio. The data points other than UA5 are estimated from references [5-29, 55, 63].

Fig. 24 The ratio of the invariant cross-sections of kaons to that of pions as a function of p_T. At 540 GeV the kaon data are from UA5 and UA2 [52] and the pion data are from UA2 [52]. The curve represents ISR data at $\sqrt{s}$=53 GeV estimated from references [25, 26].

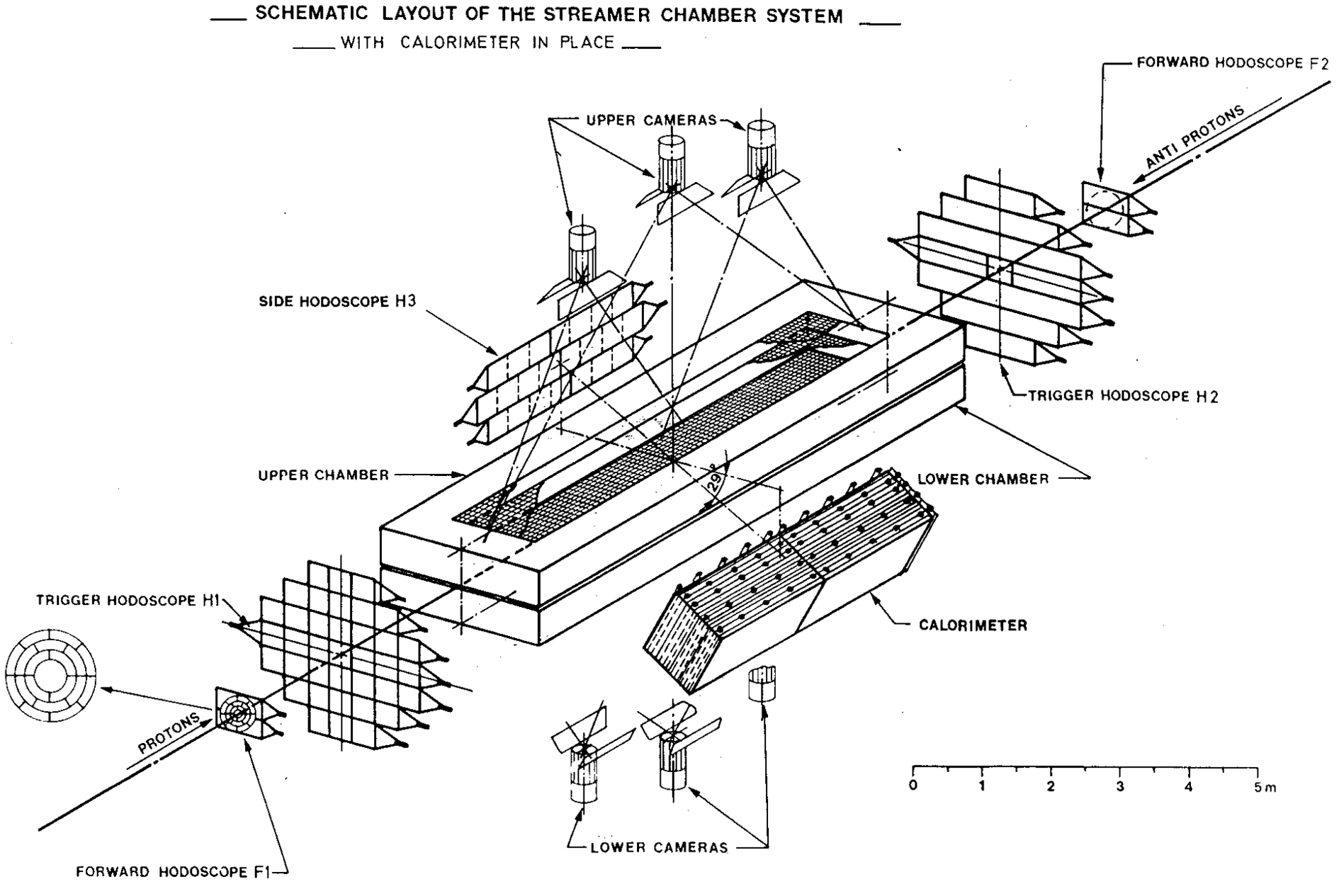
SCHEMATIC LAYOUT OF THE STREAMER CHAMBER SYSTEM
WITH CALORIMETER IN PLACE
FORWARD HODOSCOPE F2
ANTI PROTONS
UPPER CAMERAS
SIDE HODOSCOPE H3
TRIGGER HODOSCOPE H2
UPPER CHAMBER
29°
LOWER CHAMBER
TRIGGER HODOSCOPE H1
CALORIMETER
PROTONS
FORWARD HODOSCOPE F1
LOWER CAMERAS
0 1 2 3 4 5m

Fig. 1

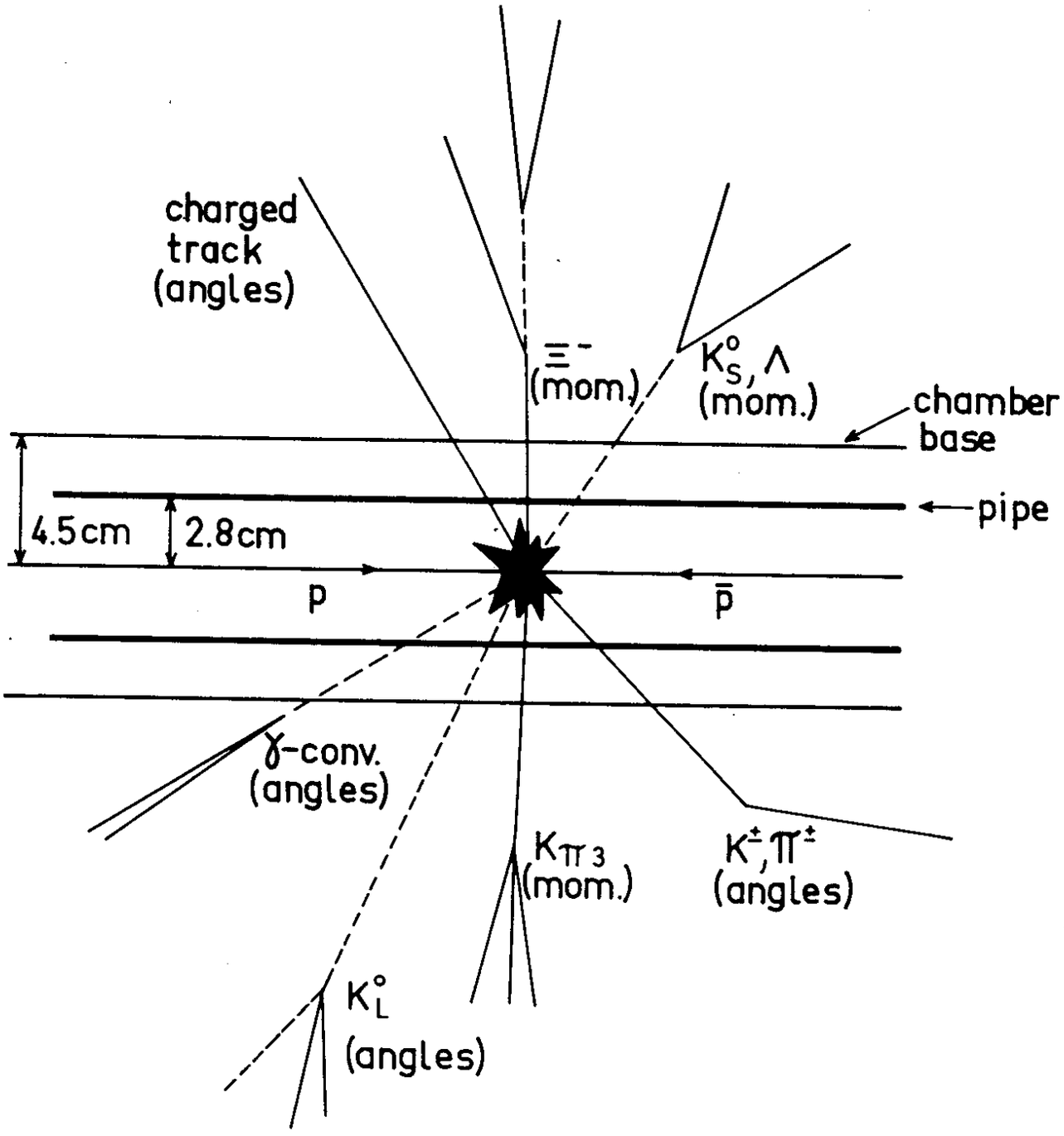
charged
track
(angles)
Ξ⁻
(mom.)
K°S, Λ
(mom.)
chamber
base
pipe
4.5cm
2.8cm
p
p̄
γ-conv.
(angles)
K°L
(angles)
Kπ3
(mom.)
K±, π±
(angles)

Fig. 2

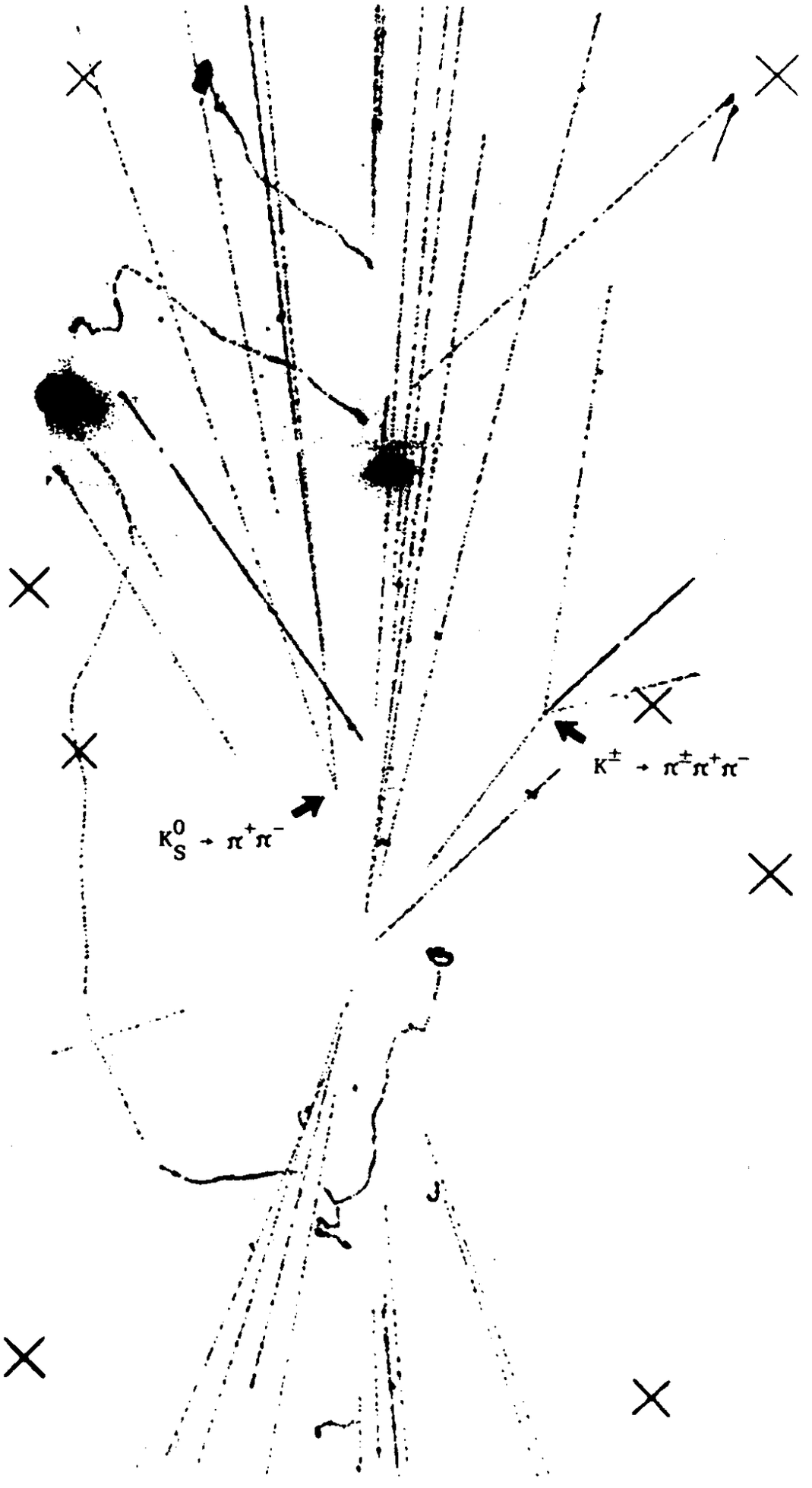

Fig. 3

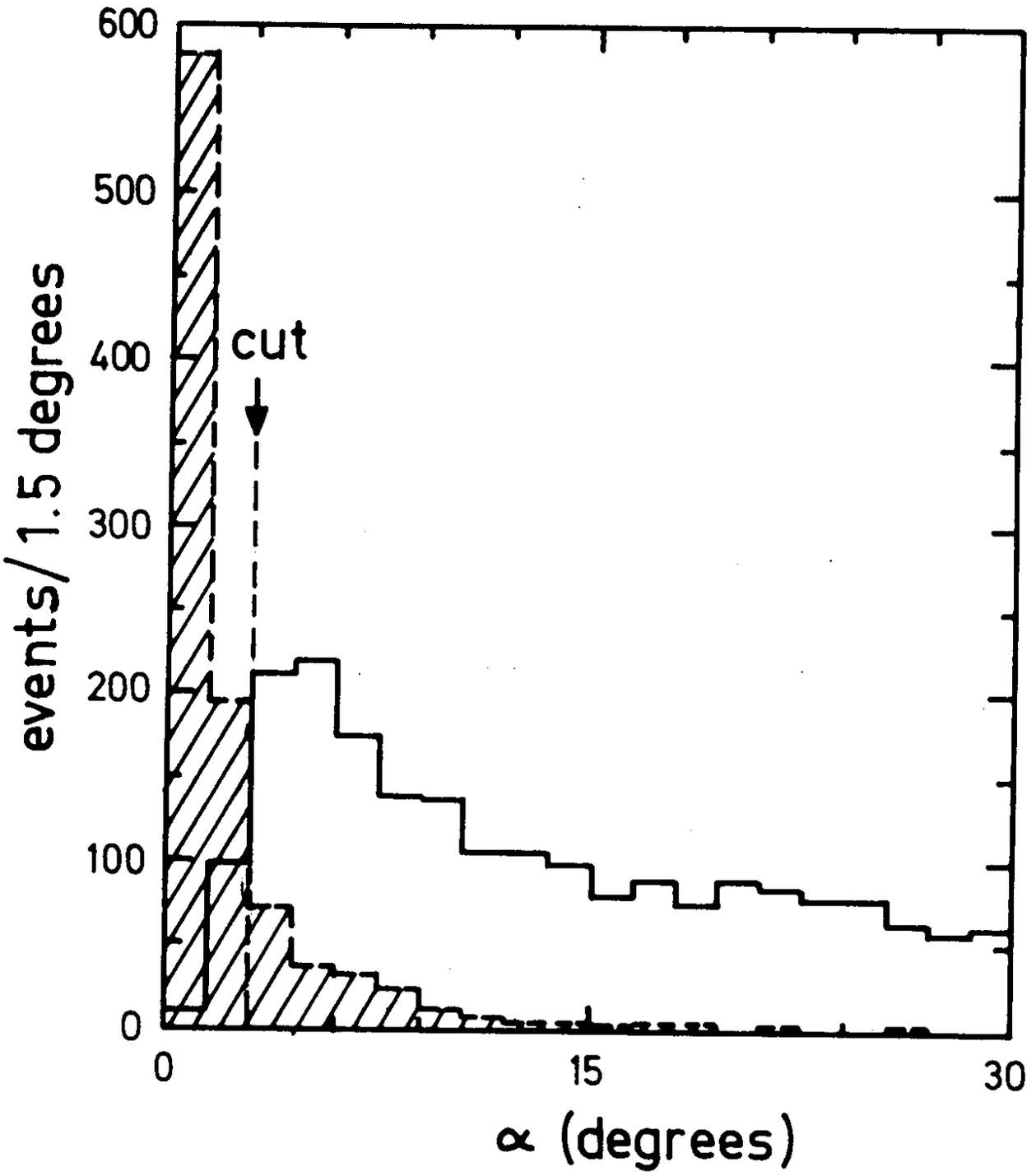
600
500
400
300
200
100
0
events/ 1.5 degrees
cut
0
15
30
α (degrees)

Fig. 4

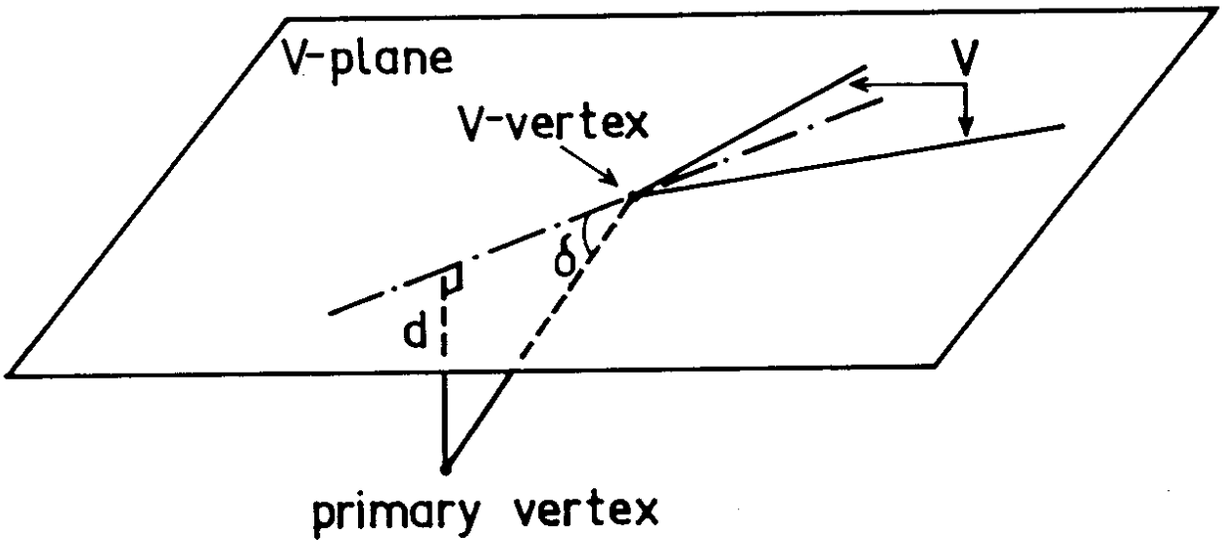

Fig. 5

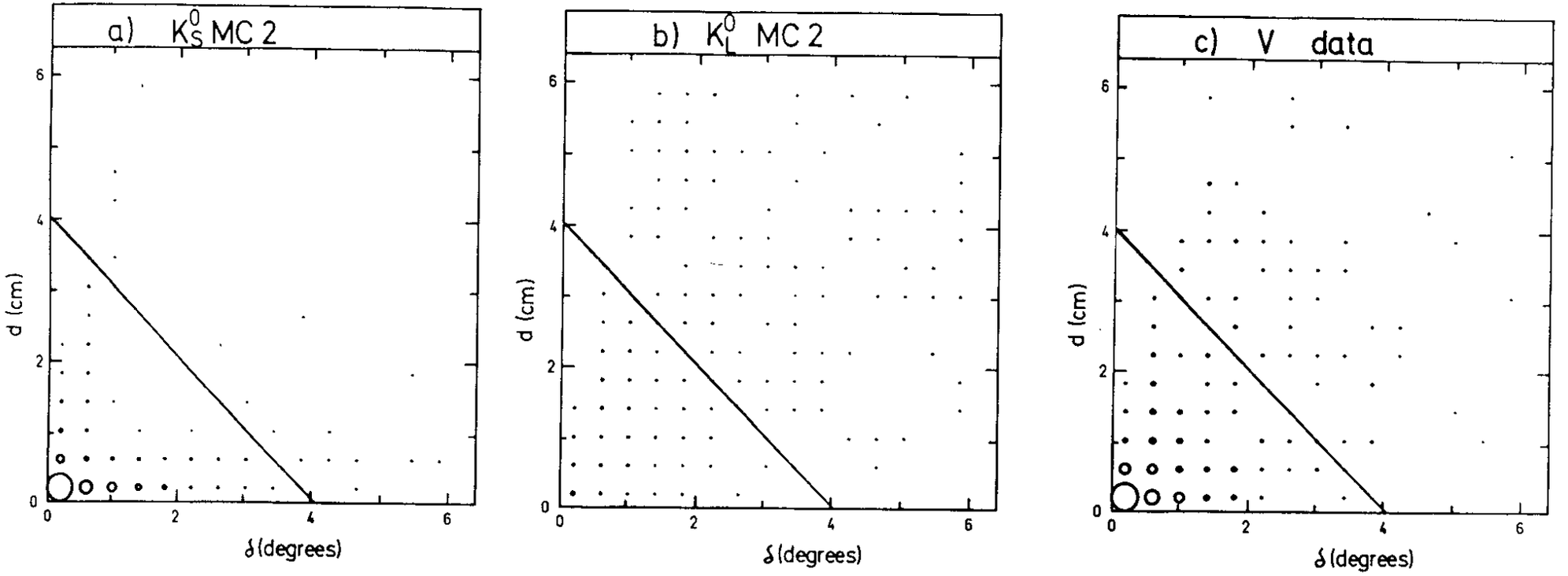

Fig. 6

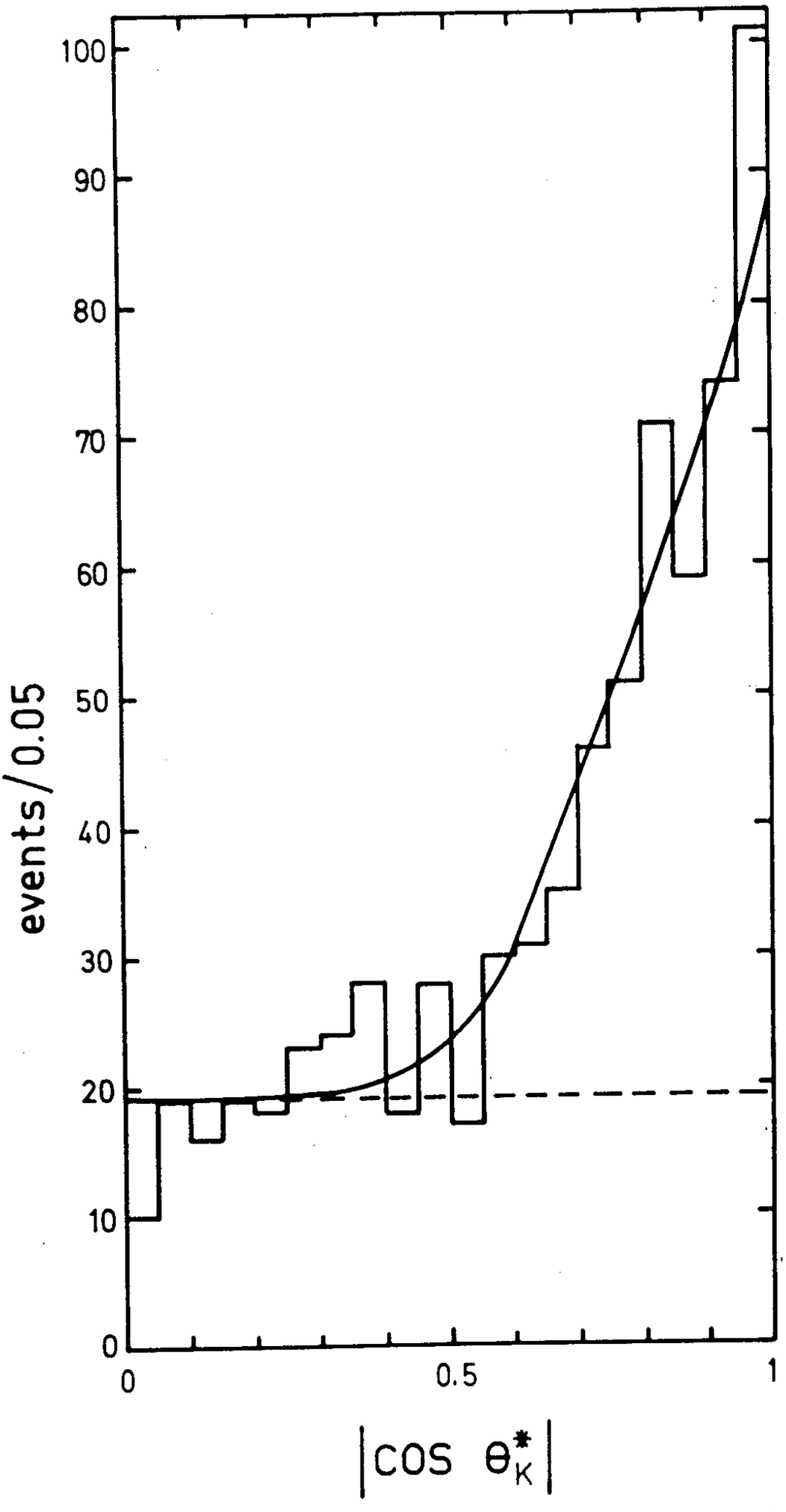

Fig. 7

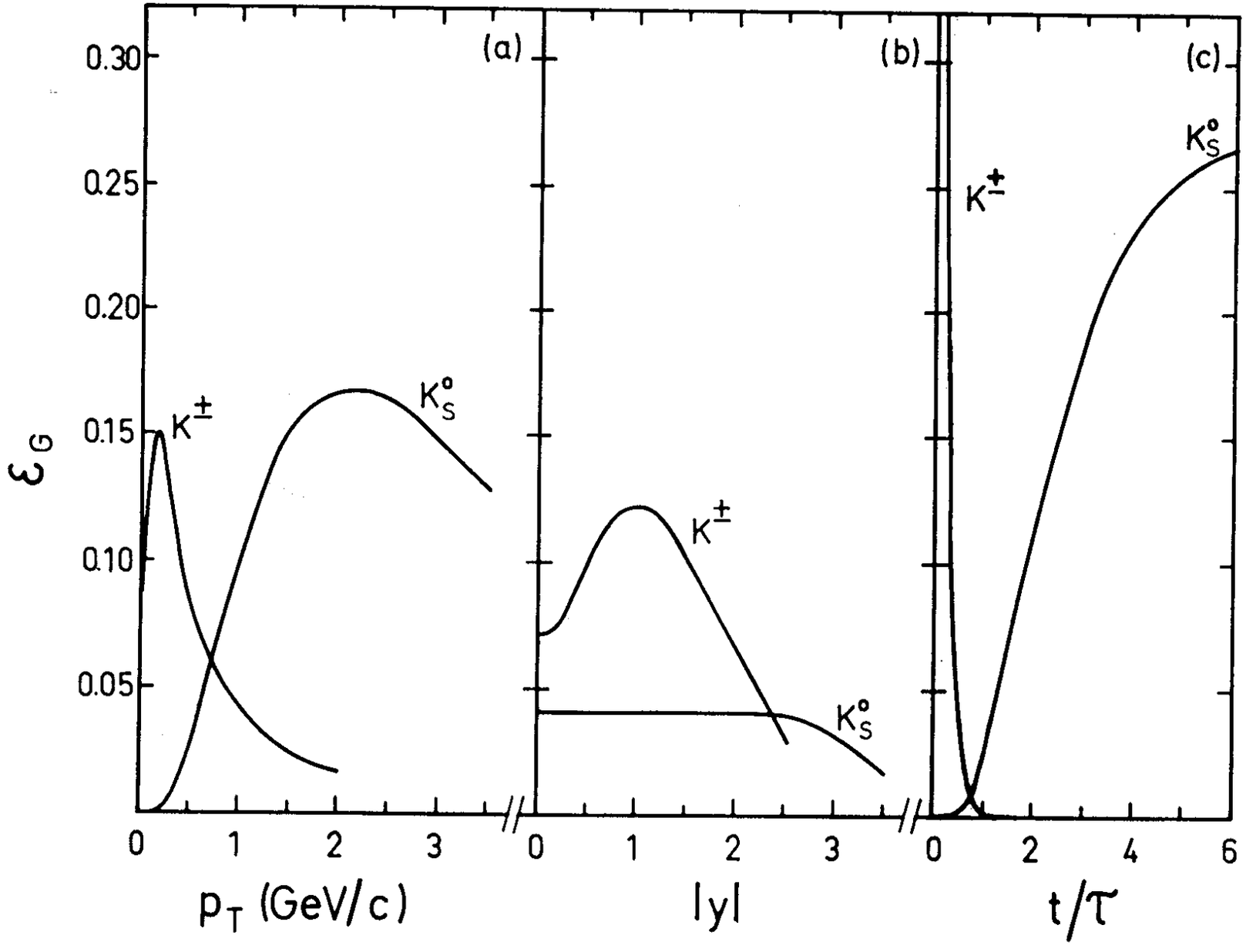
(a)
(b)
(c)
0.30
0.25
0.20
0.15
0.10
0.05
ε_G
$K^{\pm}$
K^0_S
$K^{\pm}$
K^0_S
$K^{\pm}$
K^0_S
0
1
2
3
0
1
2
3
0
2
4
6
p_T (GeV/c)
|y|
t/τ

Fig. 8

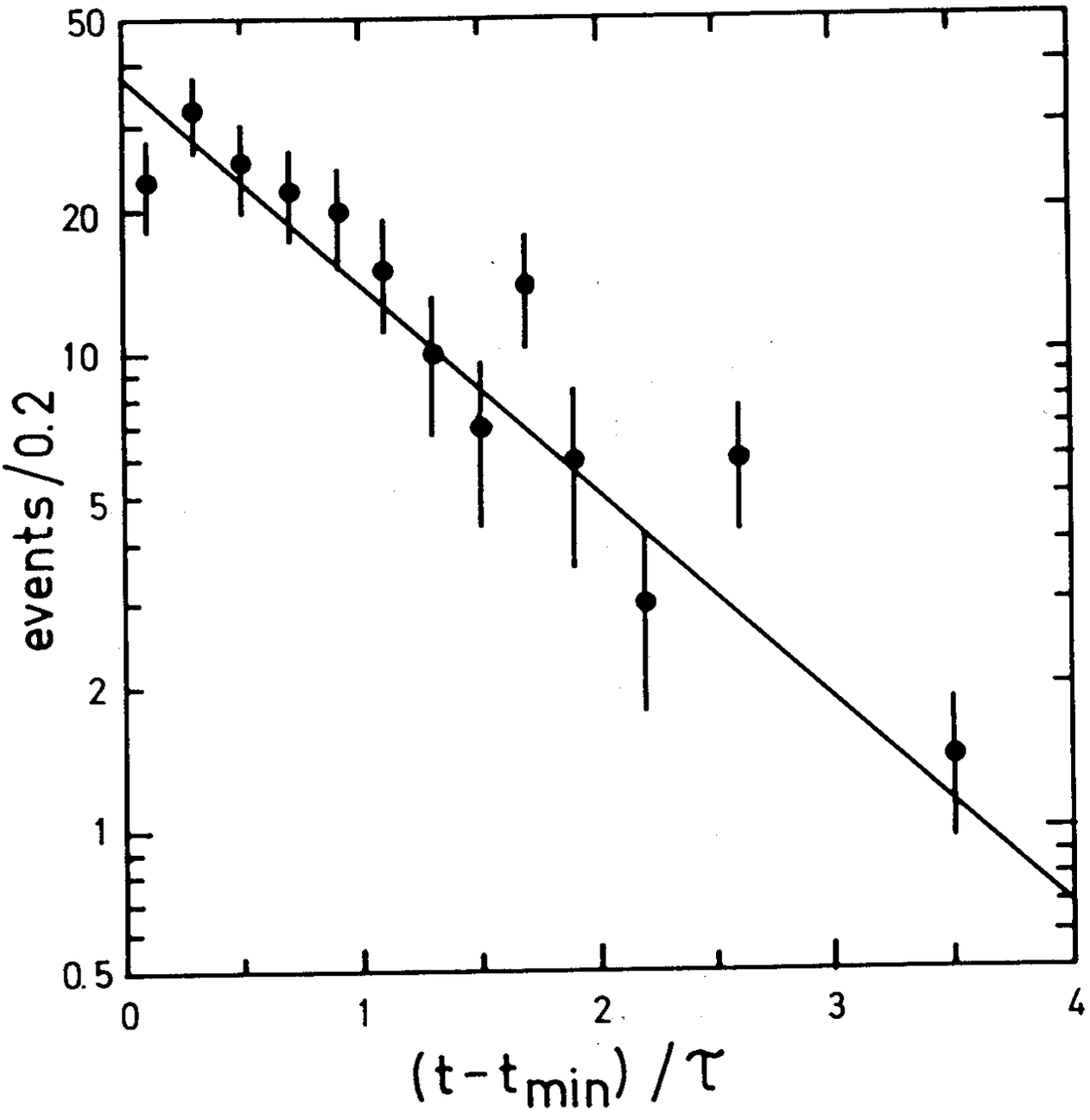

Fig. 9

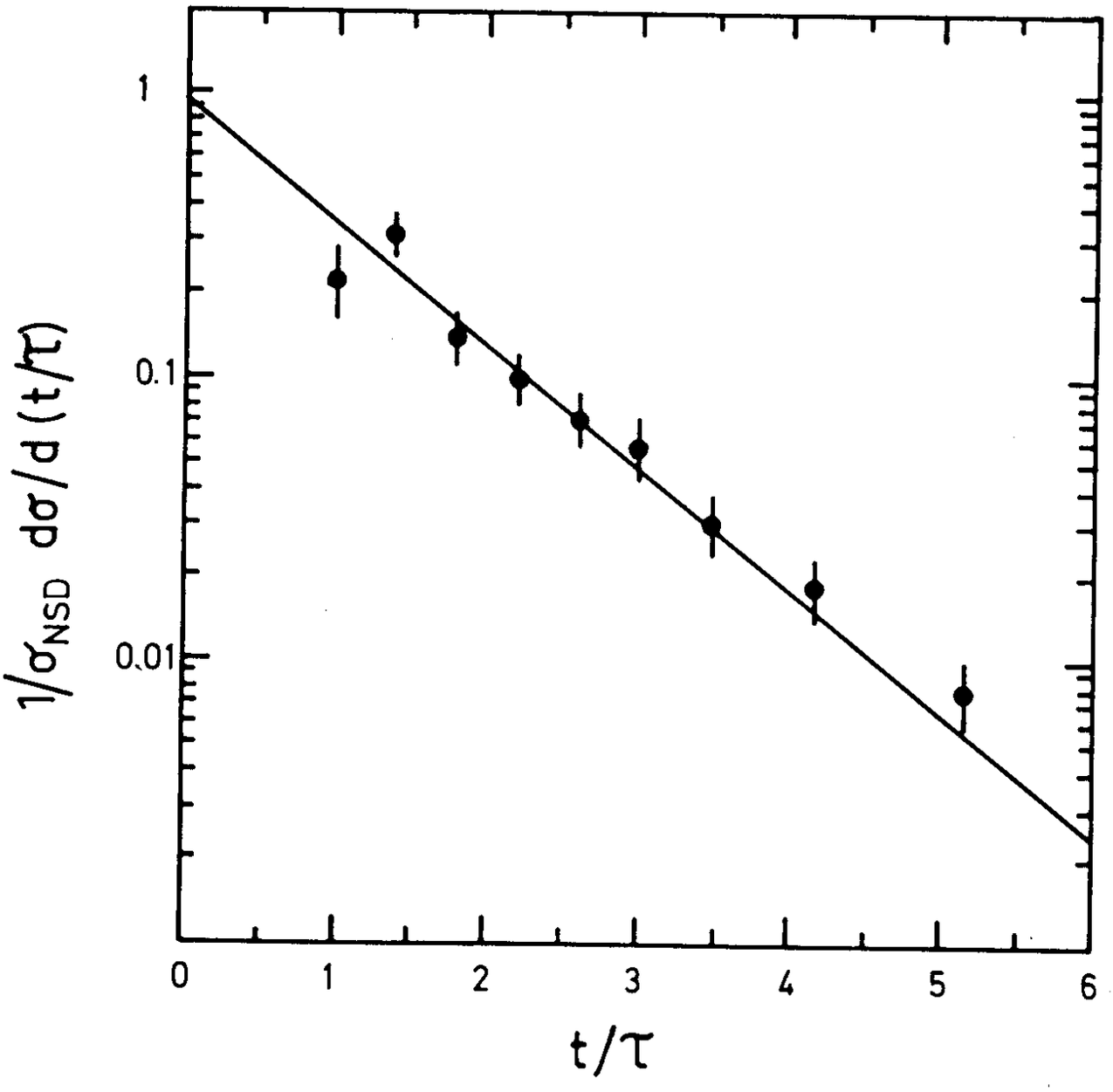

Fig. 10

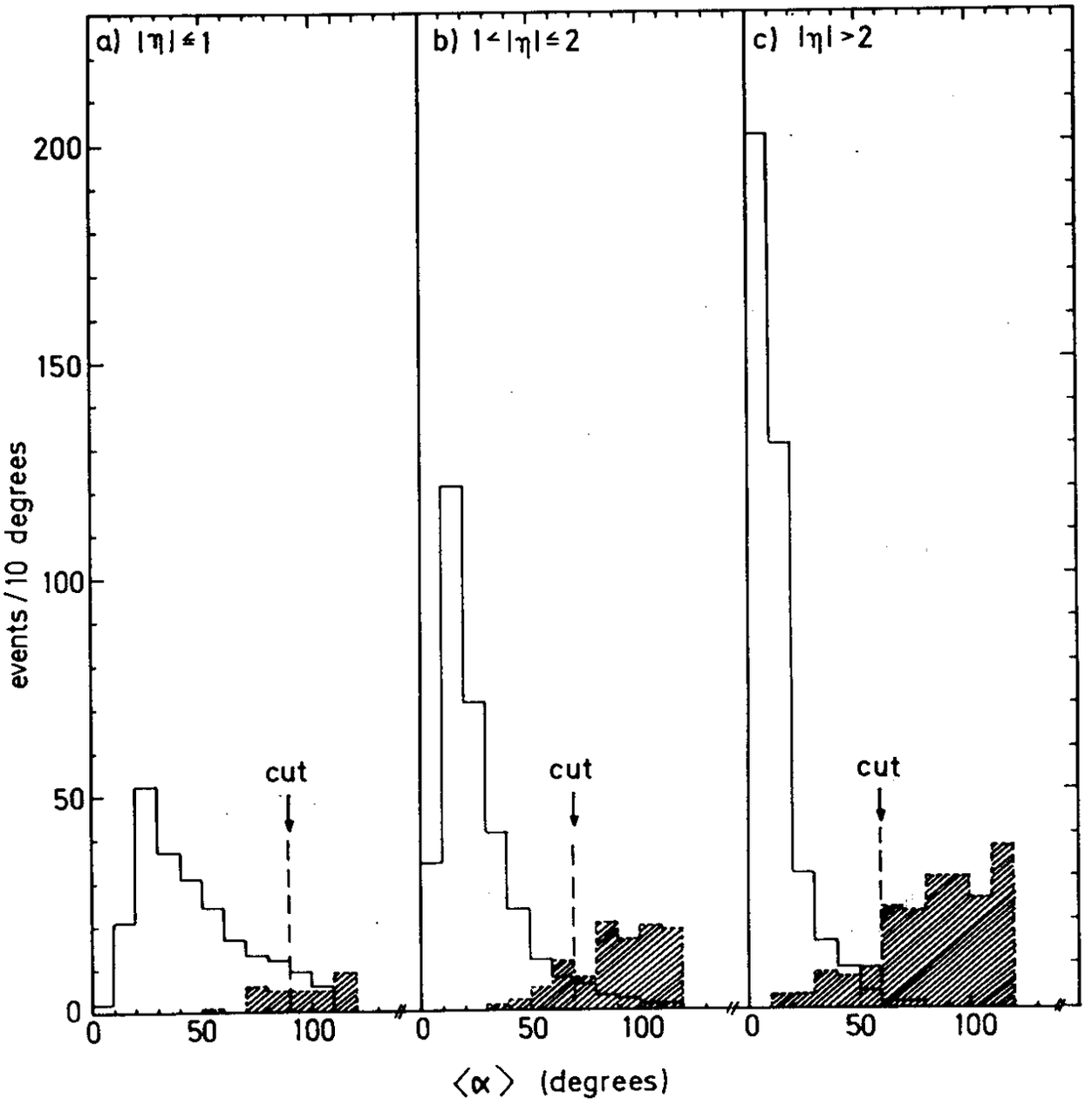
a) |η| ≤ 1
b) 1 < |η| ≤ 2
c) |η| > 2
events / 10 degrees
200
150
100
50
0
cut
cut
cut
0
50
100
0
50
100
0
50
100
⟨α⟩ (degrees)

Fig. 11

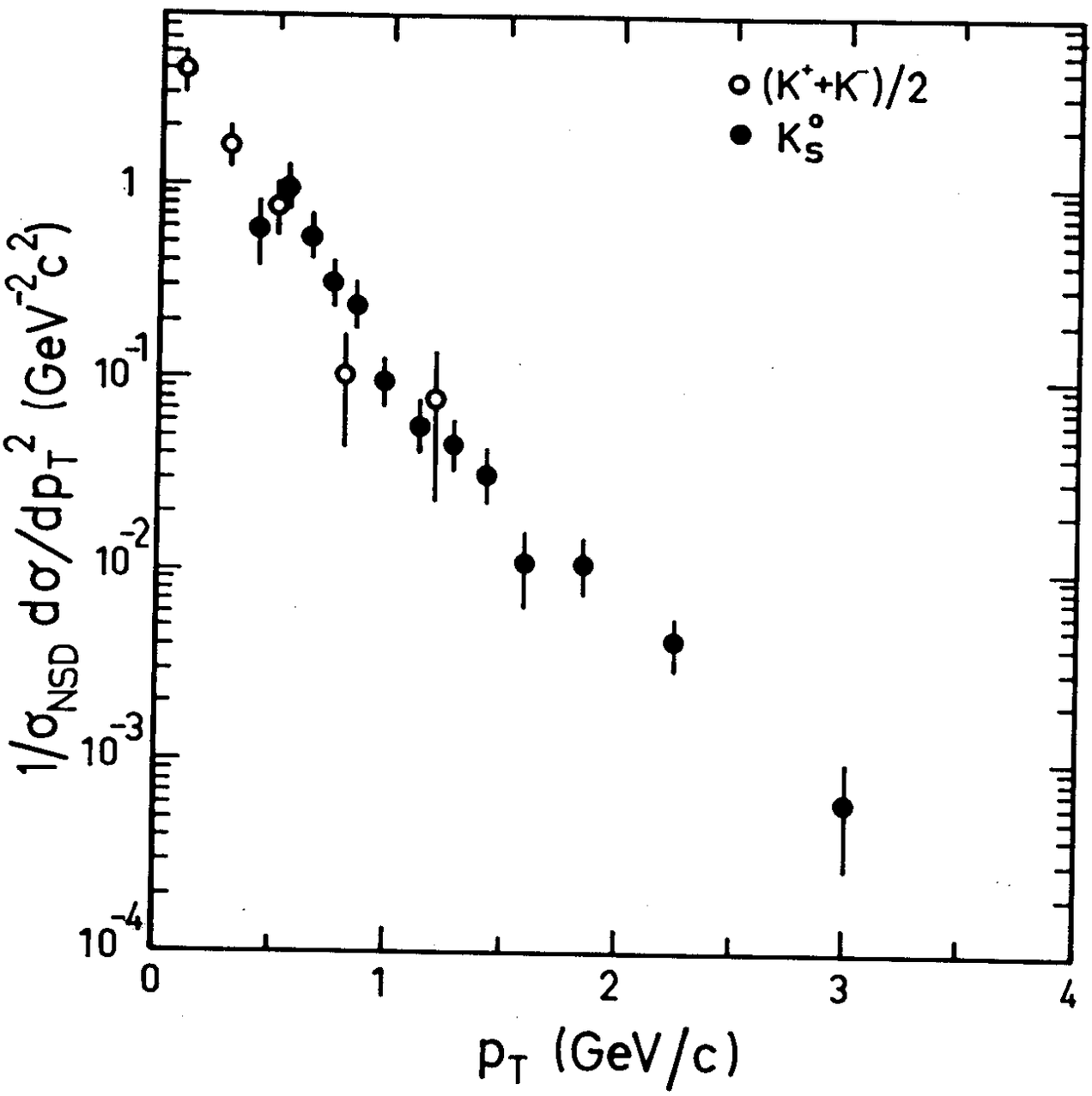

Fig. 12

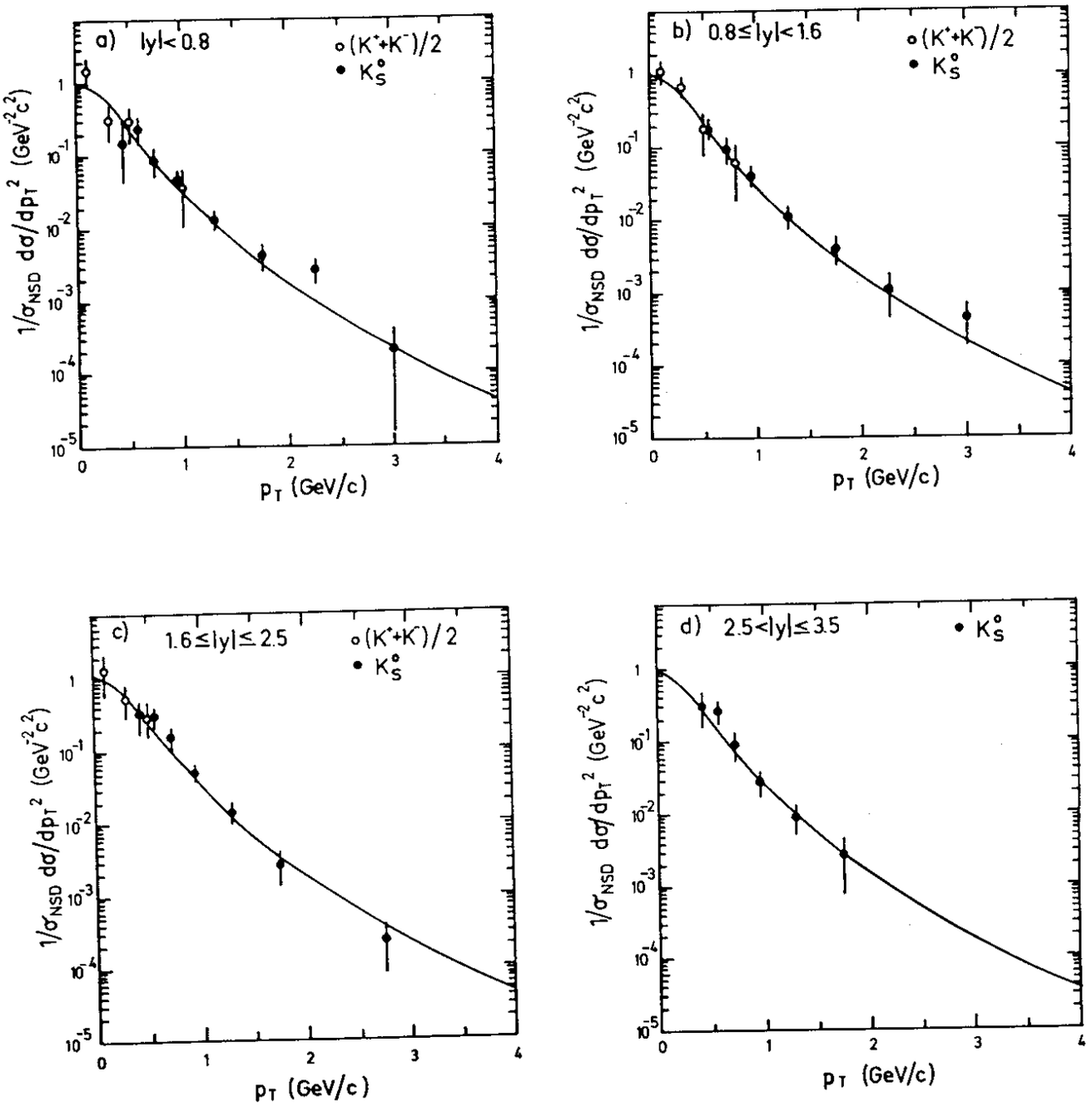
a) |y|< 0.8
o (K⁺+K⁻)/2
• K°S
b) 0.8≤|y|< 1.6
o (K⁺+K⁻)/2
• K°S
c) 1.6≤|y|≤ 2.5
o (K⁺+K⁻)/2
• K°S
d) 2.5<|y|≤3.5
• K°S
1/σNSD dσ/dpT² (GeV⁻²c²)
pT (GeV/c)

Fig. 13

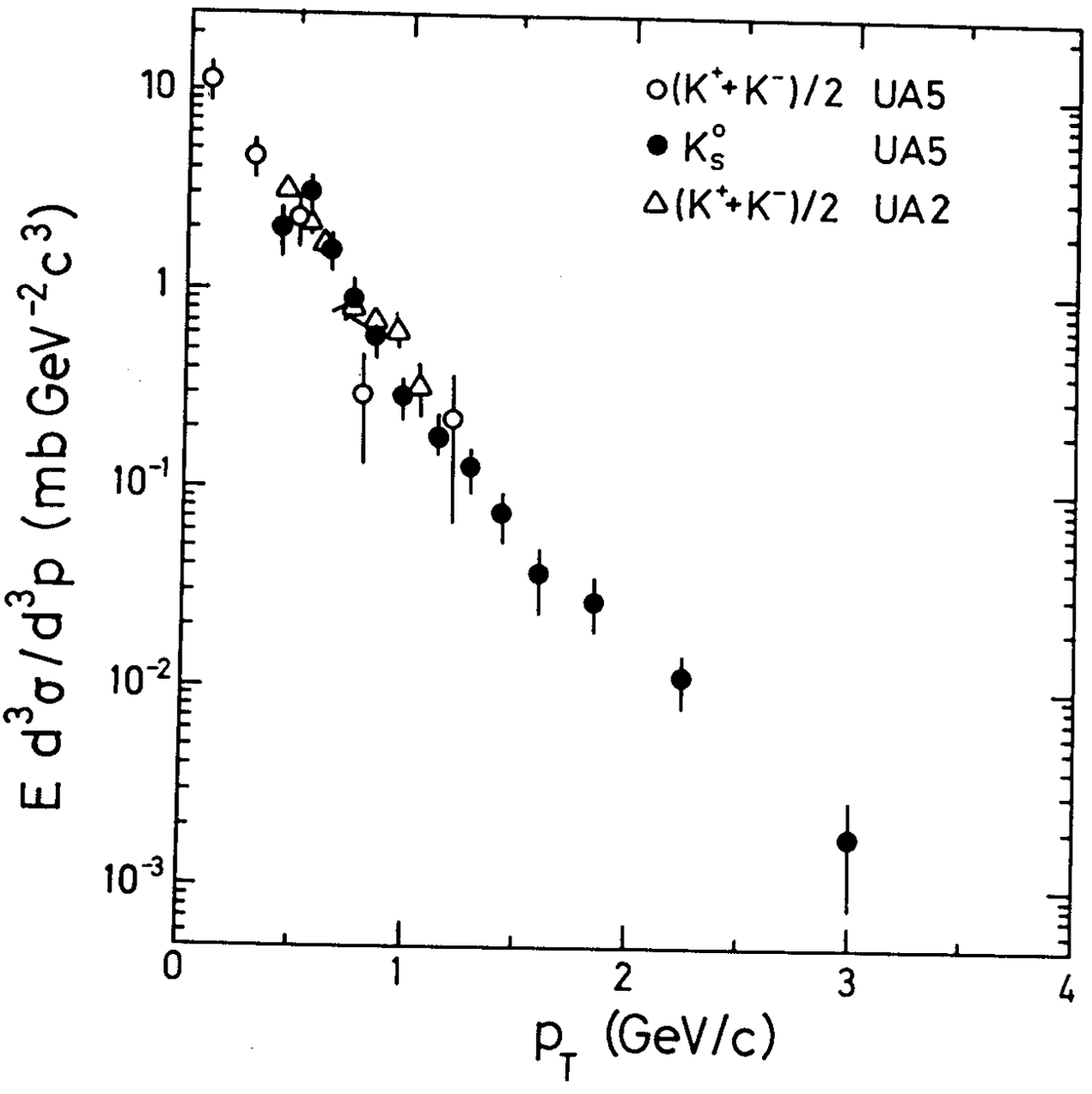
o(K⁺+K⁻)/2 UA5
● K⁰s UA5
△(K⁺+K⁻)/2 UA2
E d³σ/d³p (mb GeV⁻²c³)
10
1
10⁻¹
10⁻²
10⁻³
0
1
2
3
4
p_T (GeV/c)

Fig. 14

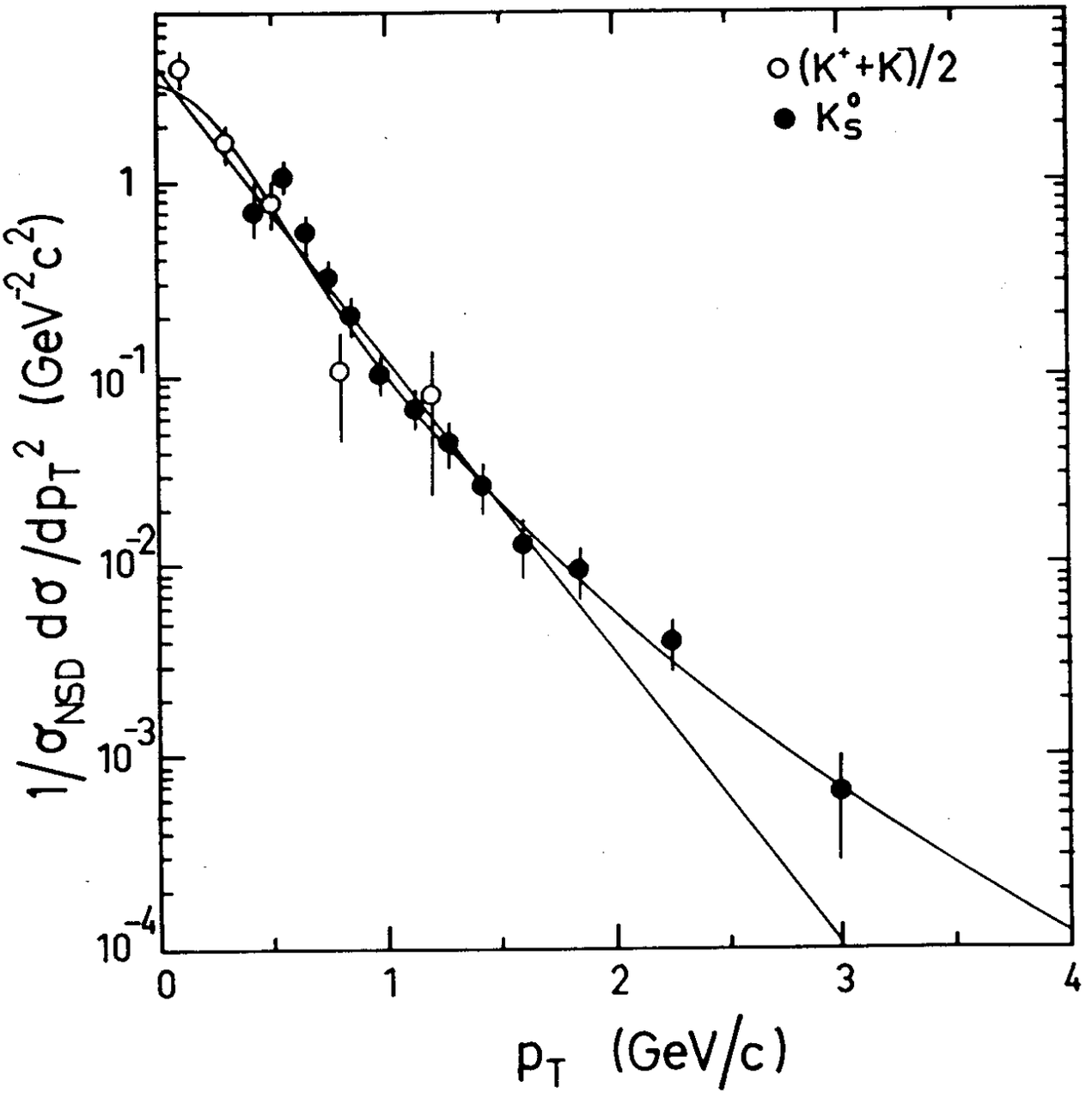

Fig. 15

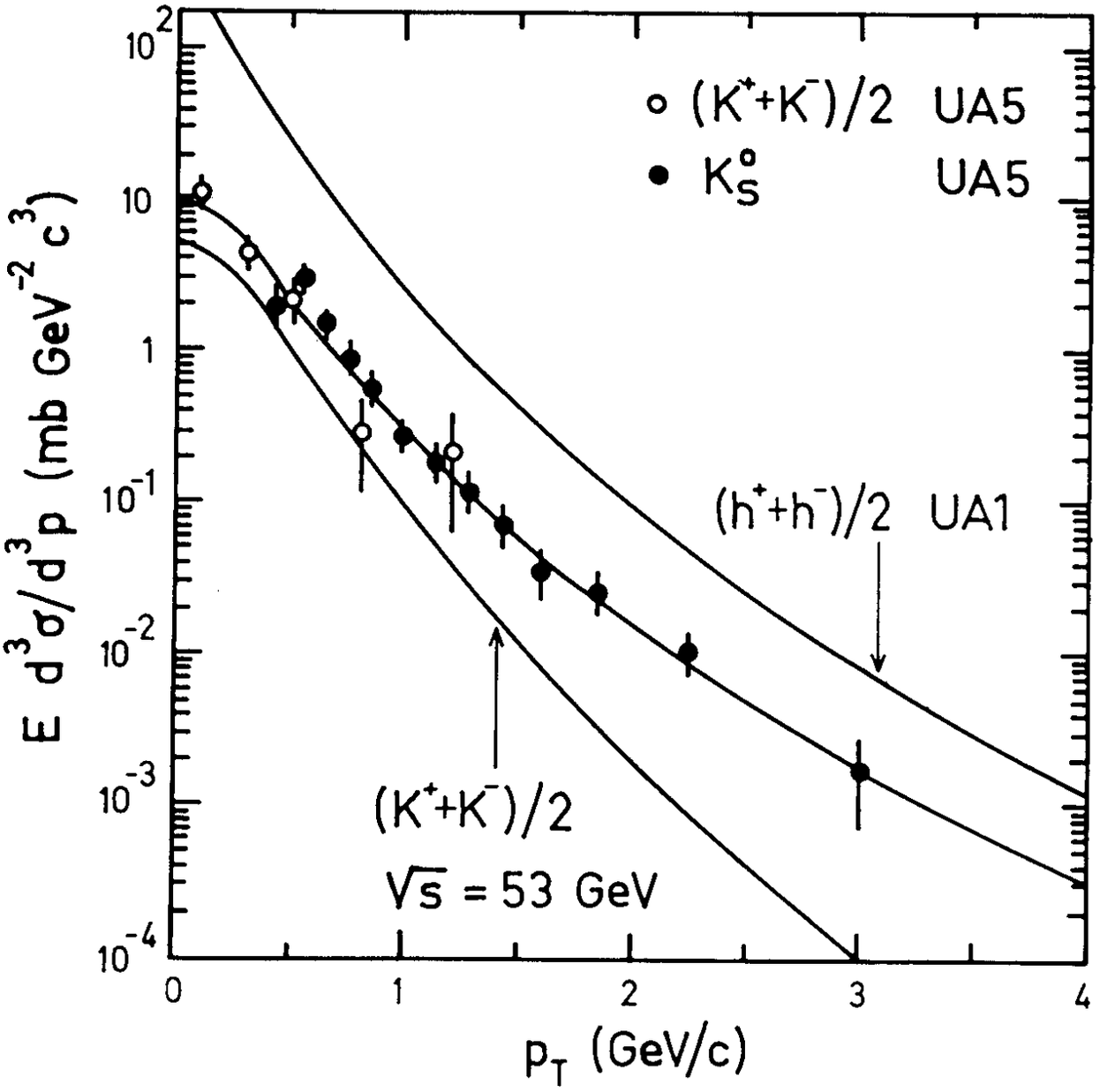
10^2
10
1
10^{-1}
10^{-2}
10^{-3}
10^{-4}
0
1
2
3
4
$E\ d^3\sigma/d^3p$ (mb GeV^{-2} c^3)
p_T (GeV/c)
o $(K^+ + K^-)/2$ UA5
• K^o_S UA5
$(h^+ + h^-)/2$ UA1
$(K^+ + K^-)/2$
$\sqrt{s}$ = 53 GeV

Fig. 16

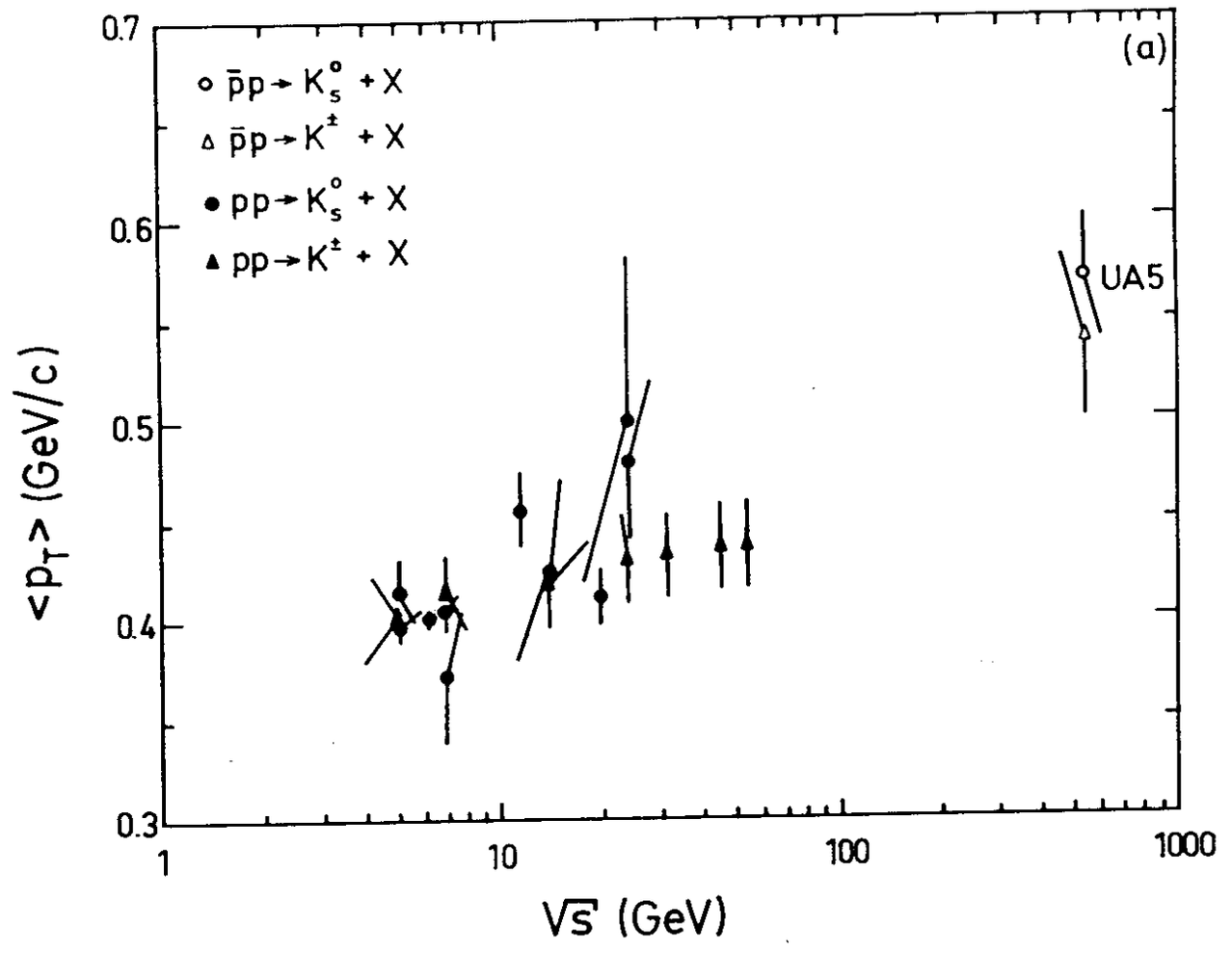
(a)
$\circ\ \bar{p}p \to K^0_s + X$
$\triangle\ \bar{p}p \to K^\pm + X$
$\bullet\ pp \to K^0_s + X$
$\blacktriangle\ pp \to K^\pm + X$
UA5
$\langle p_T \rangle$ (GeV/c)
$\sqrt{s}$ (GeV)
0.7
0.6
0.5
0.4
0.3
1
10
100
1000

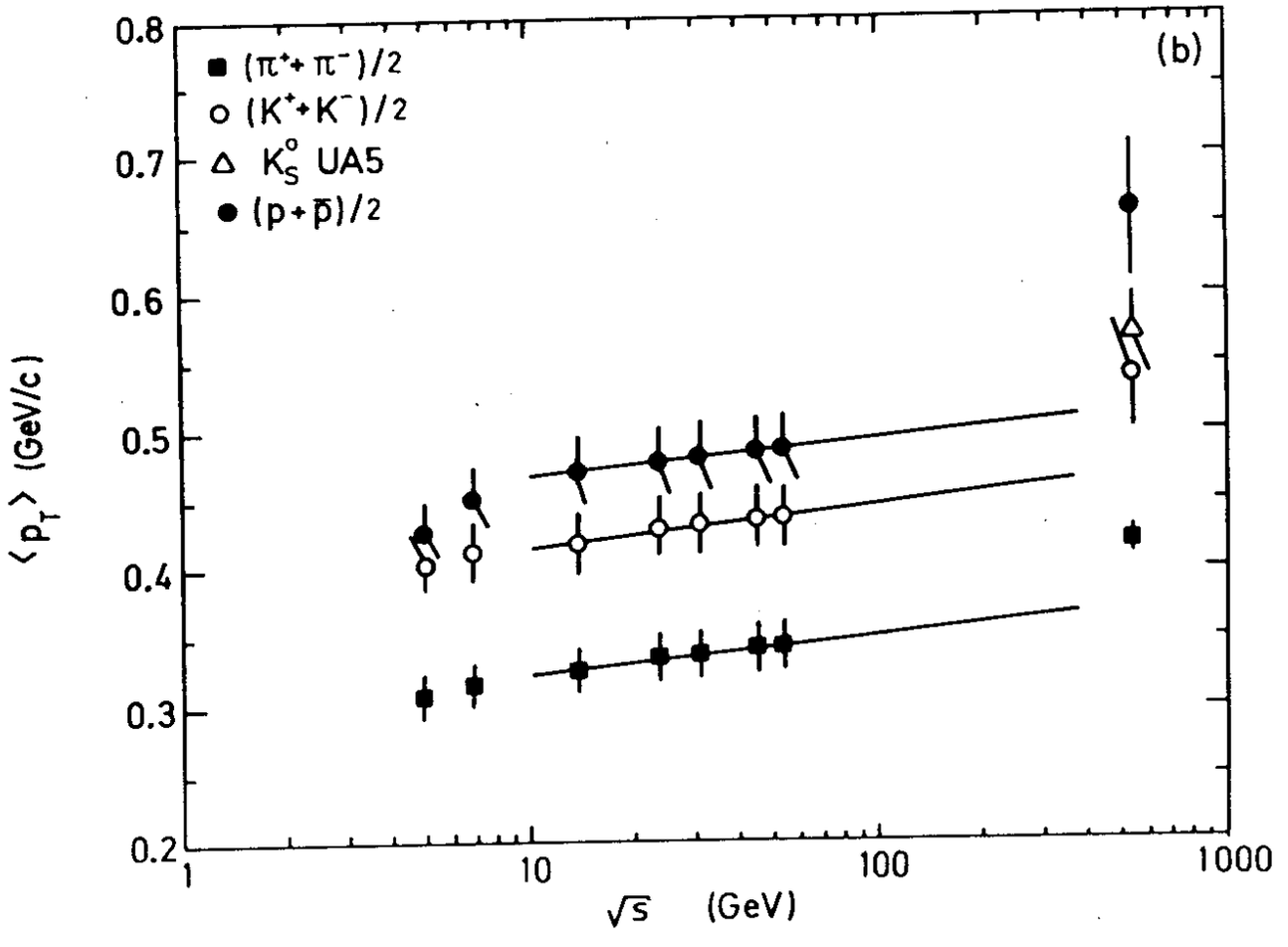
(b)
$\blacksquare\ (\pi^+ + \pi^-)/2$
$\circ\ (K^+ + K^-)/2$
$\triangle\ K^0_S$ UA5
$\bullet\ (p + \bar{p})/2$
$\langle p_T \rangle$ (GeV/c)
$\sqrt{s}$ (GeV)
0.8
0.7
0.6
0.5
0.4
0.3
0.2
1
10
100
1000

Fig. 17

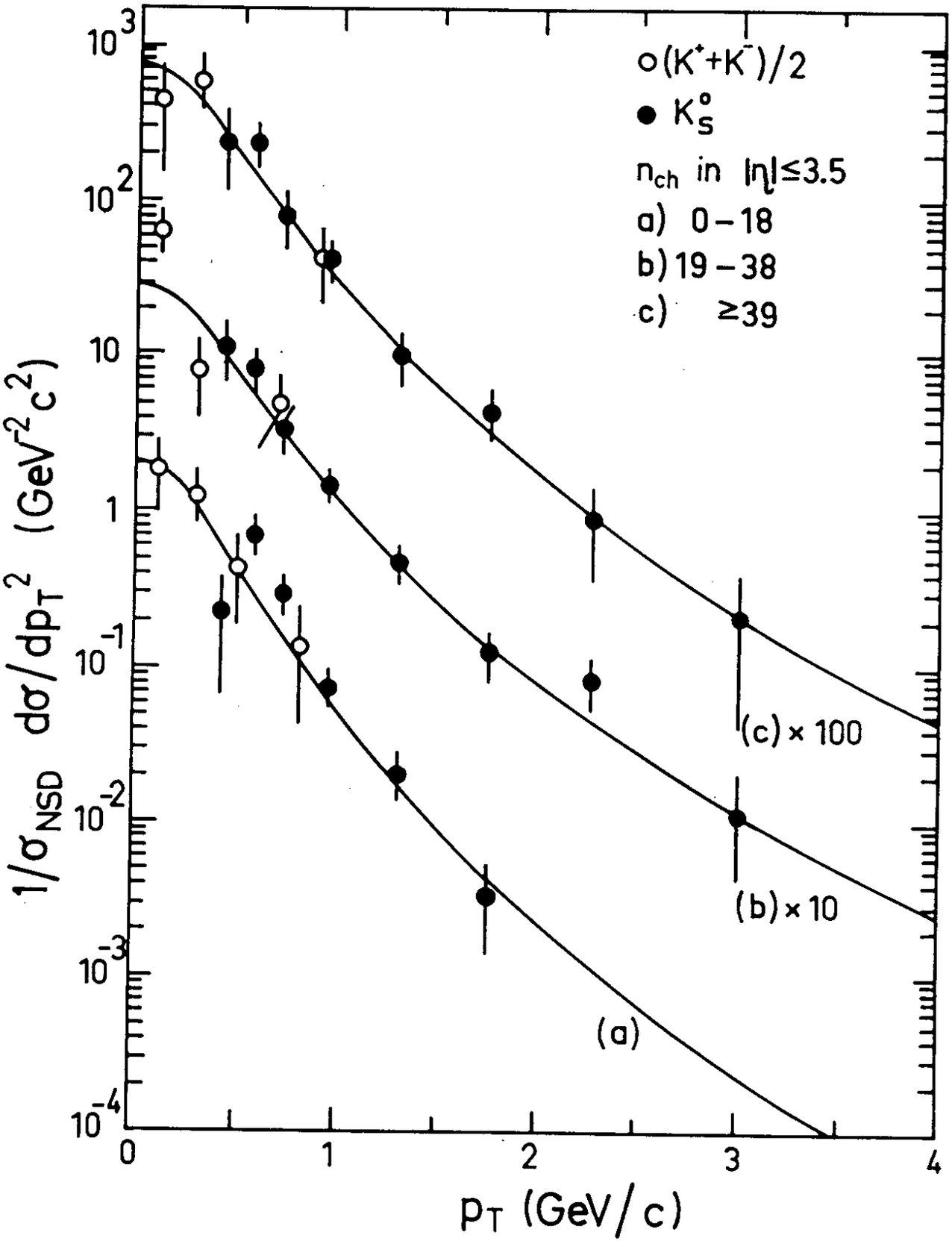
o(K⁺+K⁻)/2
● K°s
n_ch in |η|≤3.5
a) 0–18
b) 19–38
c) ≥39
(c) × 100
(b) × 10
(a)
1/σ_NSD dσ/dp_T² (GeV⁻²c²)
p_T (GeV/c)

Fig. 18

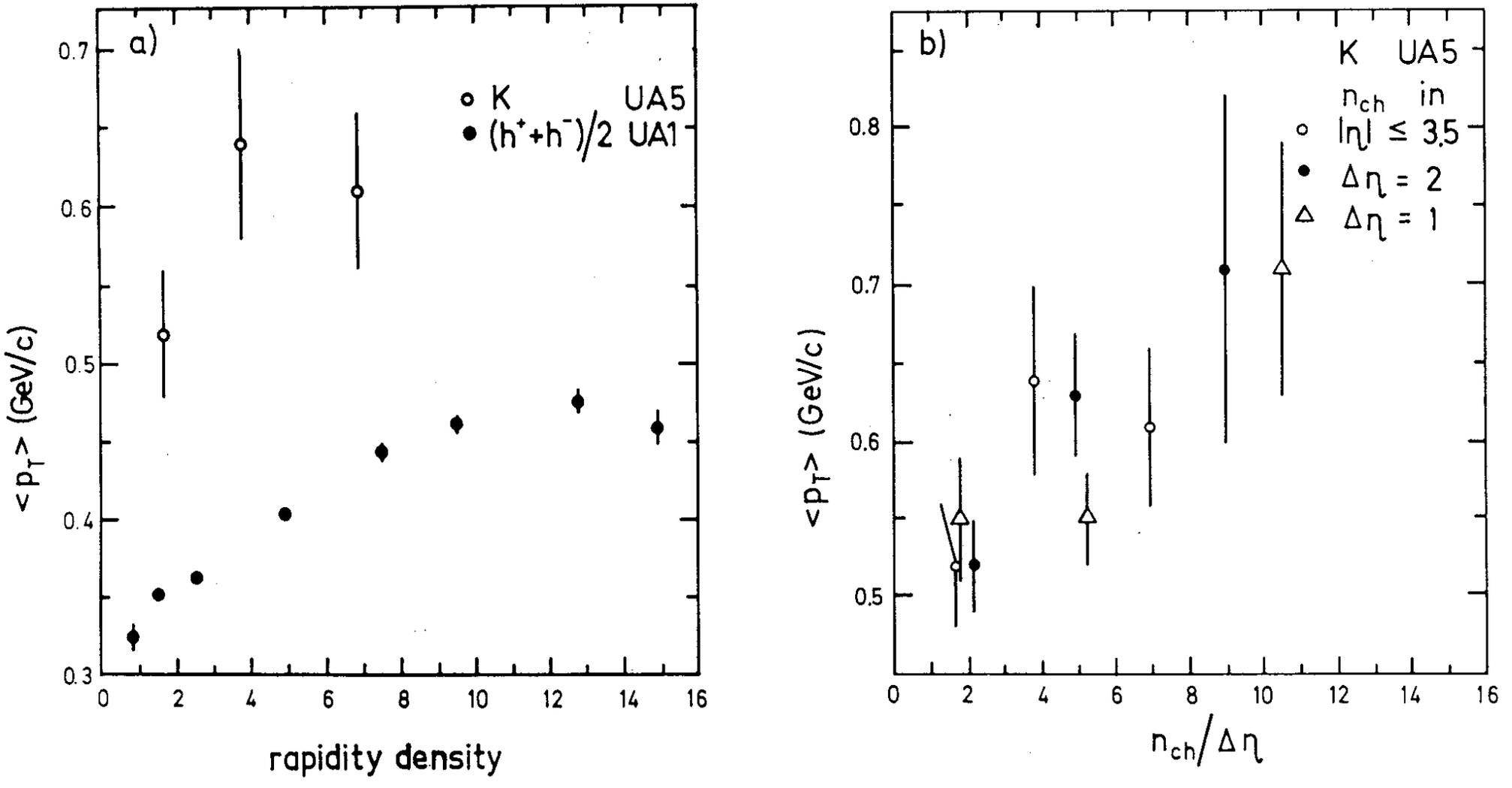
a)
K UA5
(h⁺+h⁻)/2 UA1
<pT> (GeV/c)
rapidity density
b)
K UA5
nch in
|η| ≤ 3.5
Δη = 2
Δη = 1
<pT> (GeV/c)
nch/Δη

Fig. 19

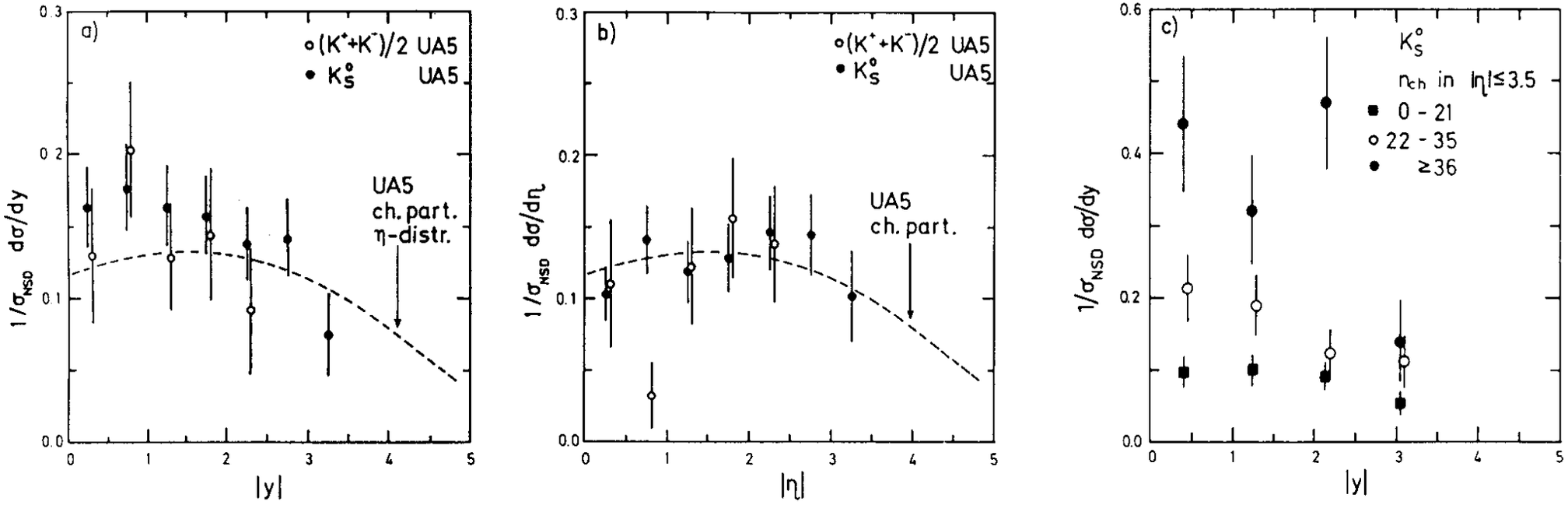
a)
o(K⁺+K⁻)/2 UA5
• K⁰S UA5
UA5
ch. part.
η-distr.
1/σNSD dσ/dy
|y|
b)
o(K⁺+K⁻)/2 UA5
• K⁰S UA5
UA5
ch. part.
1/σNSD dσ/dη
|η|
c)
K⁰S
nch in |η|≤3.5
0 - 21
22 - 35
≥36
1/σNSD dσ/dy
|y|

Fig. 20

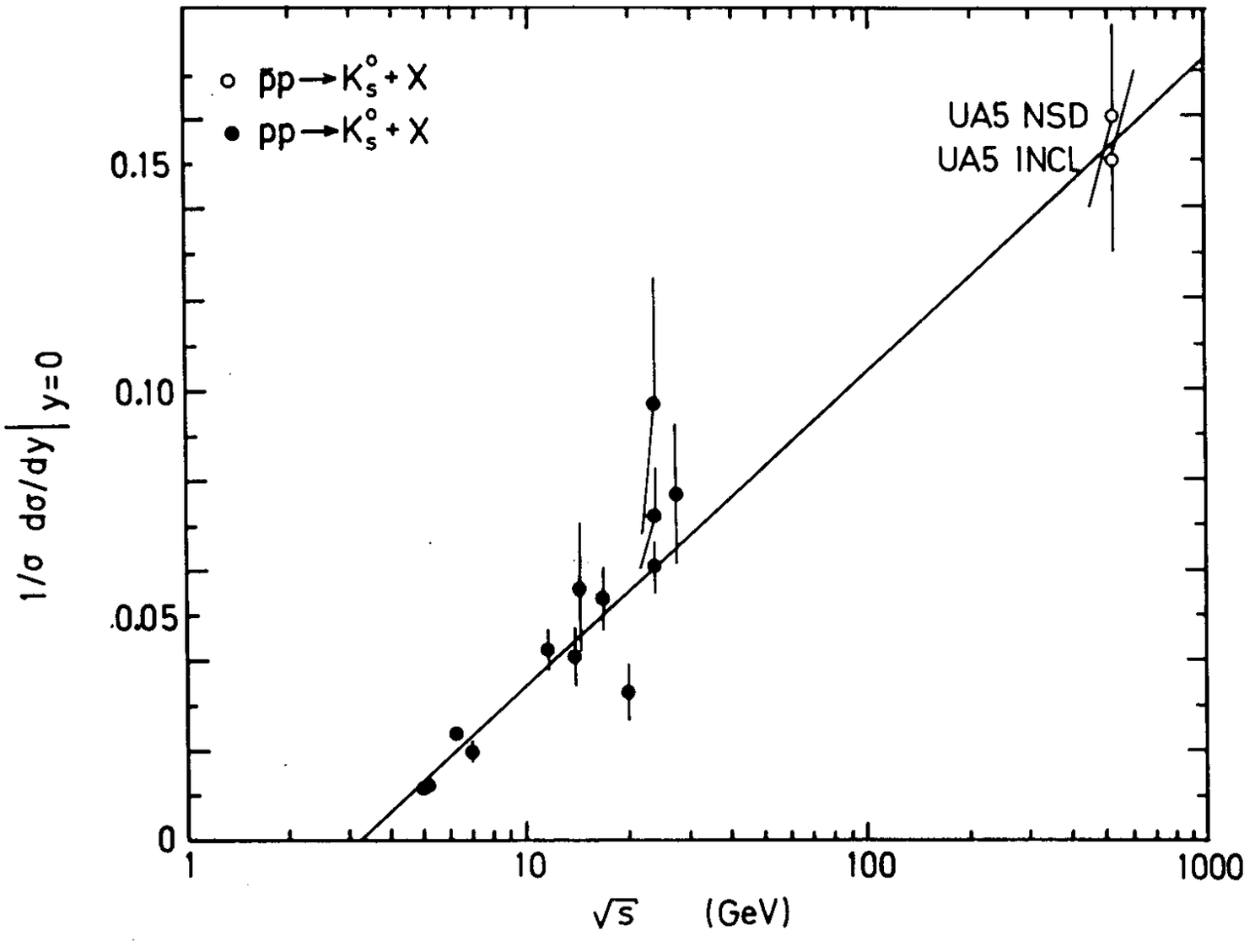
$\bar{p}p \rightarrow K^0_s + X$
$pp \rightarrow K^0_s + X$
UA5 NSD
UA5 INCL
$1/\sigma\ d\sigma/dy\big|_{y=0}$
0.15
0.10
0.05
0
1
10
100
1000
$\sqrt{s}$ (GeV)

Fig. 21

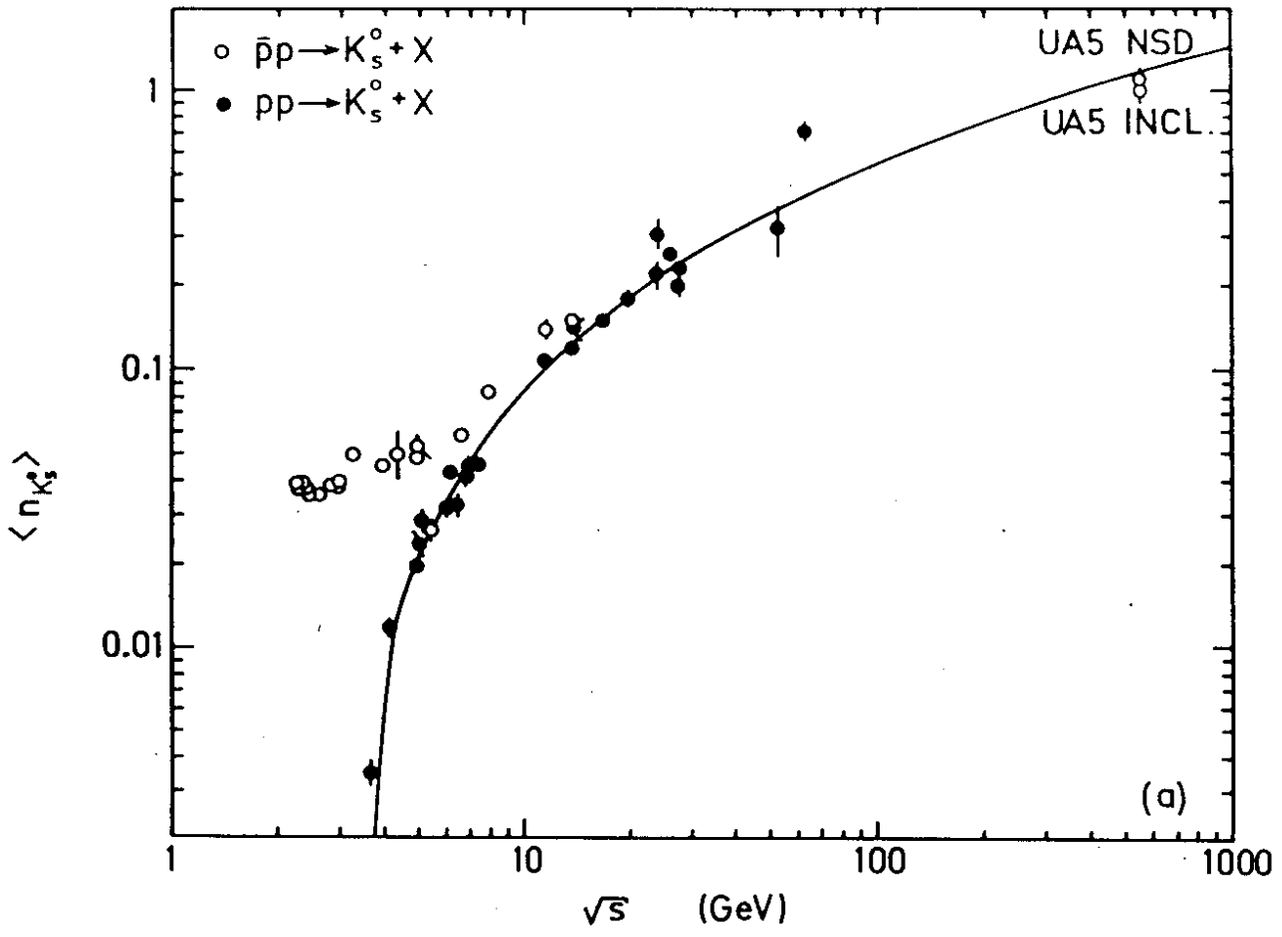
$\bar{p}p \rightarrow K^0_s + X$
$pp \rightarrow K^0_s + X$
UA5 NSD
UA5 INCL.
(a)
$\langle n_{K^0_s} \rangle$
$\sqrt{s}$ (GeV)

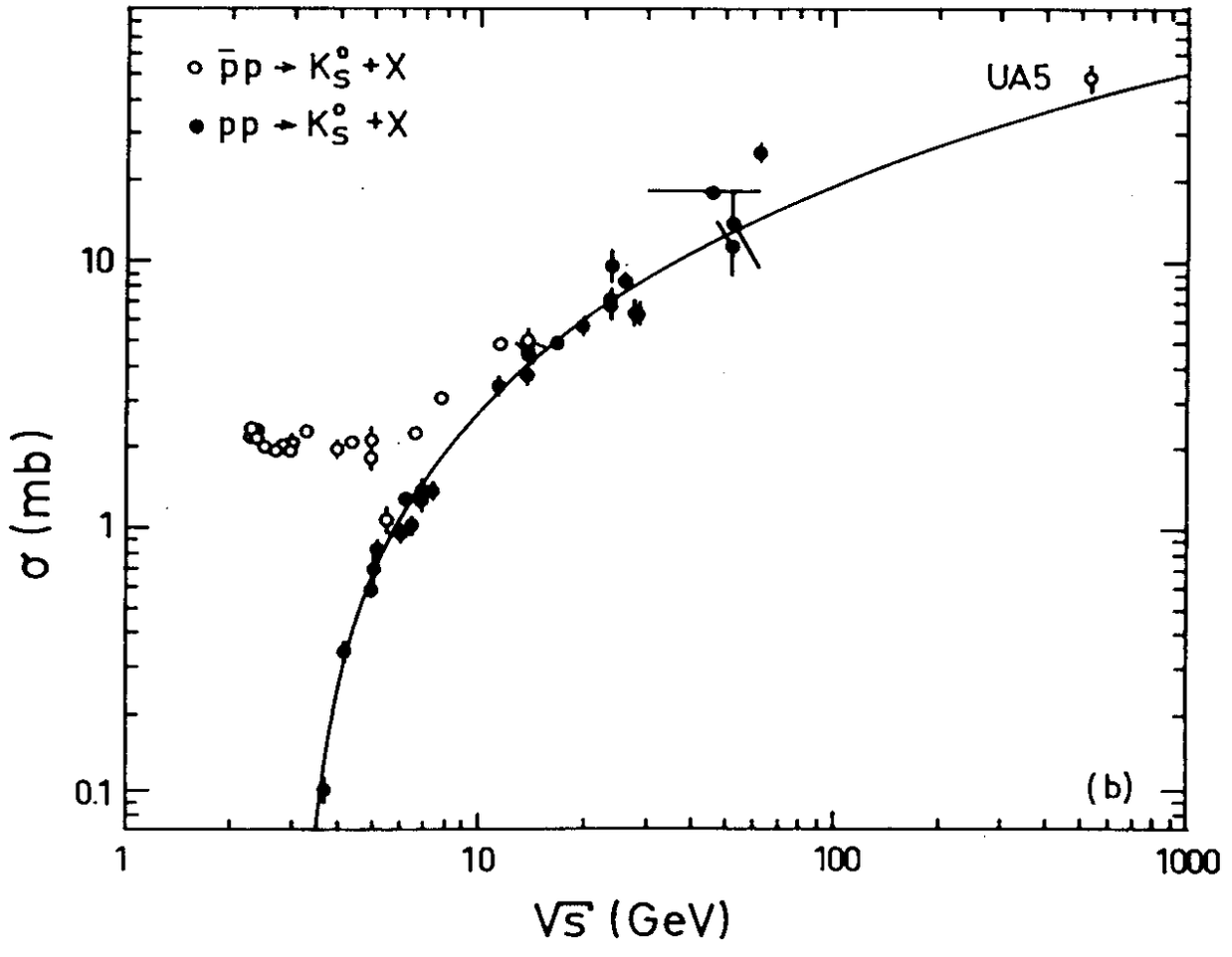
$\bar{p}p \rightarrow K^0_S + X$
$pp \rightarrow K^0_S + X$
UA5
(b)
σ (mb)
$\sqrt{s}$ (GeV)

Fig. 22

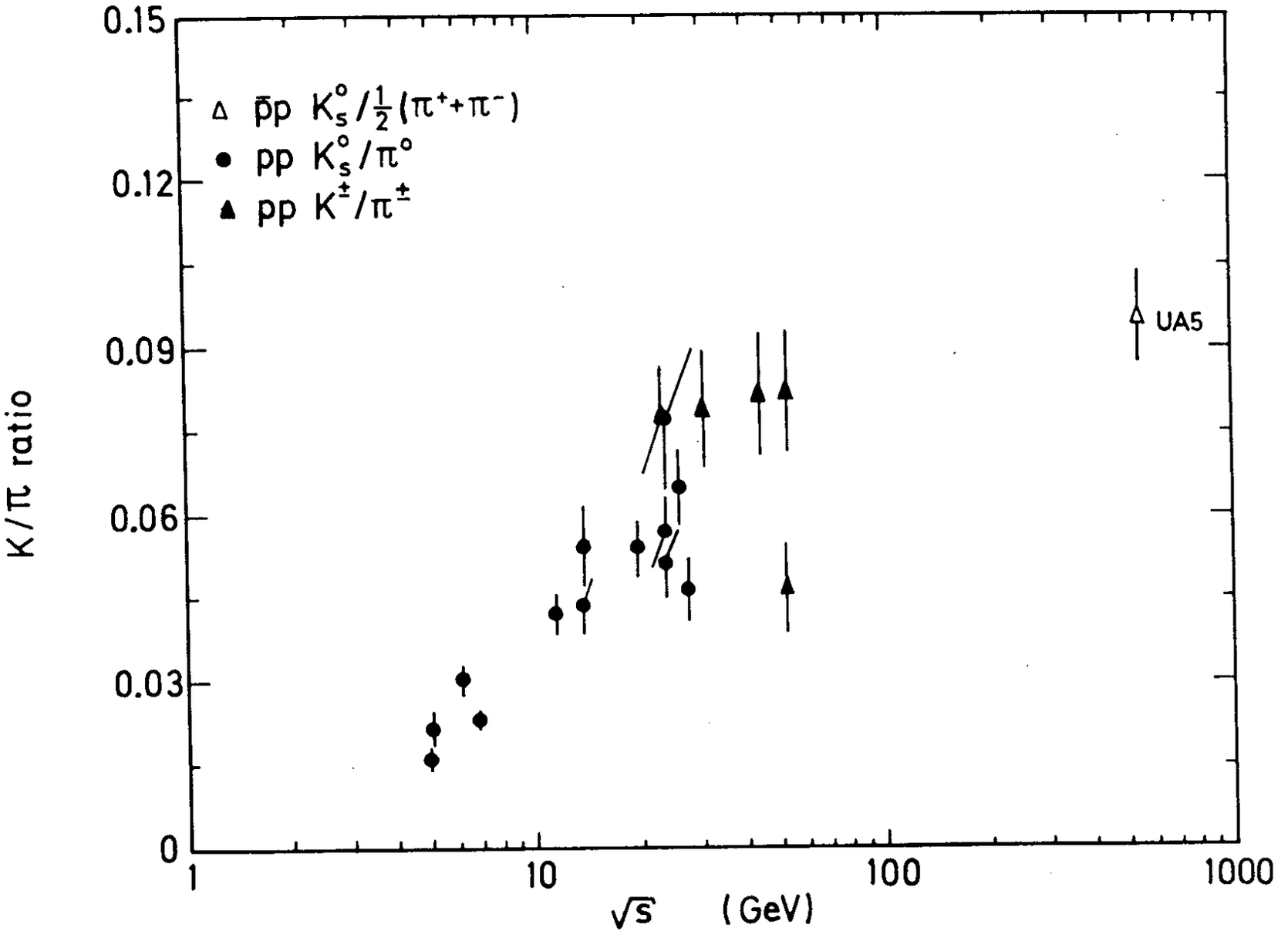
0.15
0.12
0.09
0.06
0.03
0
K/π ratio
Δ p̄p $K^0_s/\frac{1}{2}(\pi^+ + \pi^-)$
● pp K^0_s/π^0
▲ pp $K^\pm/\pi^\pm$
UA5
1
10
100
1000
√s (GeV)

Fig. 23

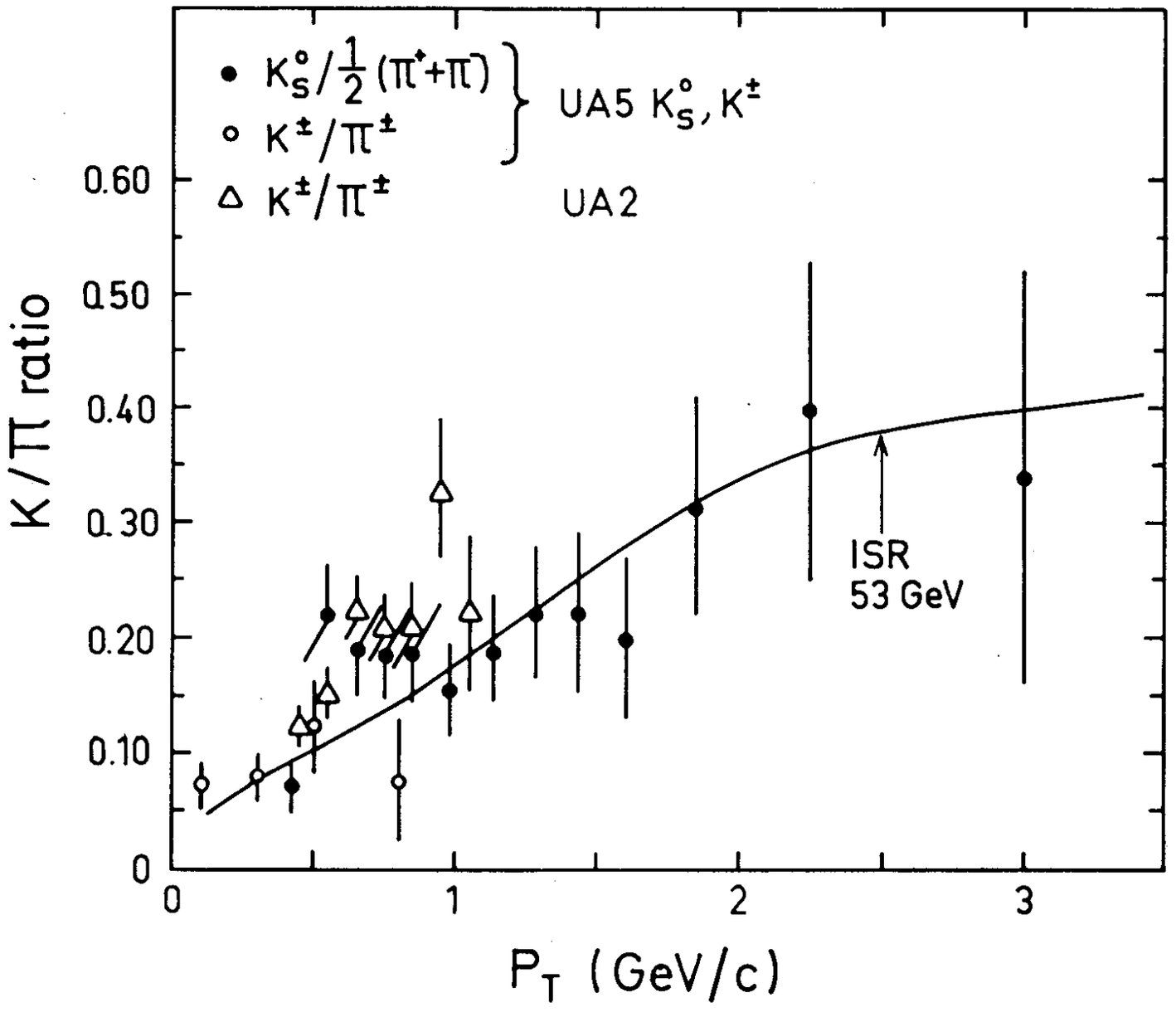
$K^0_S/\frac{1}{2}(\pi^+ + \pi^-)$
$K^\pm/\pi^\pm$
UA5 $K^0_S, K^\pm$
$K^\pm/\pi^\pm$
UA2
K/π ratio
0.60
0.50
0.40
0.30
0.20
0.10
0
0
1
2
3
ISR
53 GeV
P_T (GeV/c)

Fig. 24